Supercritical fluid extraction of essential oil from chamomile flowers: modelling, and parameter estimation

Oliwer Sliczniuk[a,*], Pekka Oinas[a]

[a]Aalto University, School of Chemical Engineering, Espoo, 02150, Finland

ARTICLE INFO

Keywords:
Supercritical extraction
Parameter estimation
Mathematical modelling

ABSTRACT

This study investigated the supercritical extraction process of chamomile extract from chamomile flowers. A distributed-parameter model describes the fluid-solid extraction process. The concept of quasi-one-dimensional flow is applied to reduce the number of spatial dimensions. The flow is assumed to be uniform across any cross-section, although the area available for the fluid phase can vary along the extractor. The physical properties of the solvent are estimated from the Peng-Robinson equation of state. Model parameters, including the partition factor, internal diffusion coefficient, axial diffusion coefficient, and decaying factor, were determined through maximum likelihood estimation based on experimental data, with the assumption of normally distributed errors. A set of laboratory experiments was performed under multiple constant operating conditions: $30 - 40°C$, $100 - 200$ bar, and $3.33 - 6.67 \times 10^{-5}$ kg/s.

1. Introduction

This study investigates the extraction of essential oil from chamomile flowers (Matricaria chamomilla L.) via supercritical fluid extraction techniques and modelling of this process. Chamomile is a medicinal herb widely cultivated in southern and eastern Europe—such as Germany, Hungary, France, and Russia. It can be found outside of Europe in Brazil as discussed by Singh et al. [1]. This plant is distinguished by its hollow, bright gold cones, housing disc or tubular florets and surrounded by about fifteen white ray or ligulate florets. Chamomile has been used for its medicinal benefits, serving as an anti-inflammatory, antioxidant, mild astringent, and healing remedy. Chamomile's aqueous extract is widely used as a gentle sedative to calm nerves and mitigate anxiety, hysteria, nightmares, insomnia, and other sleep-related conditions, according to Srivastava [2]. Orav et al. [3] reported that oil yields from dried chamomile samples ranged from 0.7 to 6.7 mL kg^{-1}. Notably, the highest yields of essential oil, between 6.1 and 6.7 mL kg^{-1}, were derived from chamomile sourced from Latvia and Ukraine, while chamomile from Armenia exhibited a lower oil content of 0.7 mL kg^{-1}.

Evaluating the economic viability of the process is essential when choosing the suitable technology for essential oil extraction. Traditional methods, such as distillation and organic solvent extraction, are commonly employed but come with drawbacks. Distillation, for example, involves high temperatures that can lead to the thermal degradation of heat-sensitive compounds. This limitation has led to the increased popularity of alternative techniques like supercritical fluid extraction. Supercritical carbon dioxide is particularly appealing due to its distinctive properties: it's inflammable, non-toxic, has a low critical temperature, and is non-corrosive. Moreover, its relatively low critical point, compared to other fluids, positions it as an advantageous alternative to conventional extraction methods. Supercritical fluids are capable of exhibiting both gas- and liquid-like properties, allowing for adjustable dissolving power through changes in operating conditions.

The literature offers a variety of mathematical models aimed at detailing the extraction of valuable compounds from a fixed biomass bed. Selecting a fitting model necessitates a deep understanding of the physical processes at play within the operational unit, as each model is built on specific assumptions and outlines distinct mass transfer mechanisms and equilibrium dynamics.

One model proposed by Reverchon et al. [4] is the hot ball model, which is based on an analogy to heat transfer and describes an extraction process from solid particles containing small quantities of solute where solubility is not a limiting factor.

The Broken-and-Intact Cell model, proposed by Sovova [5], assumes that external surfaces of particles are mechanically disrupted, allowing the solvent's access to the solute in broken cells, while the solute in intact cells remains less accessible due to higher mass transfer resistance.

Reverchon [6] formulated a fluid-solid extraction model where the solute is treated as a single component, governed by internal mass transfer resistance and omitting the effects of external mass transfer, axial dispersion, and variations in fluid density and flow rate throughout the bed.

This work builds upon the linear kinetic model suggested by Reverchon [6], deriving fundamental governing equations to develop a comprehensive model for the chamomile oil extraction process. This model aims for control-oriented simplicity, assuming a semi-continuous operation within a cylindrical vessel. The process involves supercritical solvent being pumped through a fixed bed of finely chopped biomass to extract the solute, followed by separation of the solvent and solute in a flush drum to collect the extract. Parameters such as the feed flow rate (F_{in}) and

*Corresponding author
oliwer.sliczniuk@aalto.fi (O. Sliczniuk)
ORCID(s): 0000-0003-2593-5956 (O. Sliczniuk); 0000-0002-0183-5558 (P. Oinas)

inlet temperature (T_{in}) are adjustable and measurable, as is the vessel pressure (P), whereas the outlet temperature (T_{out}) can only be monitored. A simplified flow diagram is presented in Figure 1, illustrating the process setup.

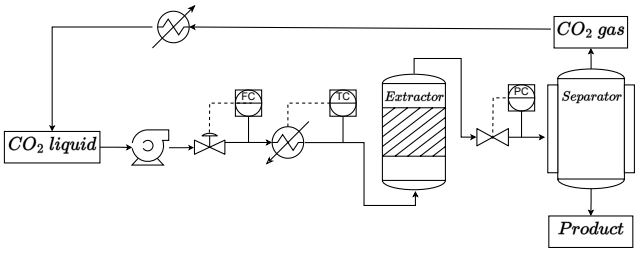

Figure 1: Process flow diagram

This study focuses on creating a process model for the extraction of natural substances from solid materials using supercritical fluids, with a particular emphasis on supercritical CO_2. The approach involves estimating the solvent properties through thermodynamic relationships and determining the extraction kinetic parameters via a series of experiments conducted under a variety of conditions. The maximum likelihood estimator method is employed to address the parameter estimation challenge, with the derived parameters subsequently used to establish correlations. These correlations are instrumental in extending the applicability of the process model across different temperatures (30 to 40°C) and pressures (100 to 200 bar).

The organization of the study is as follows: Chapter 2.1 offers an overview of supercritical fluids, aiming to acquaint the reader with their unique properties. Chapter 2.2 outlines the fundamental balance equations. These equations are then integrated with the extraction kinetic equation in Chapter 2.3 to formulate the process model. Chapter 2.4 introduces the maximum likelihood estimation technique, which is subsequently applied within the context of the process model. Chapter 2.5 details the experimental procedures and the data acquisition necessary for estimating the kinetic parameters related to the extraction process. The study culminates in Chapters 3 and 4, where the parameter estimations and simulation outcomes are thoroughly analysed and discussed.

2. Materials and methods

2.1. Supercritical fluids

A supercritical fluid (SCF) is a substance at a temperature and pressure above its critical point, where there are no distinct liquid and gas phases but below the pressure required to compress it into a solid. SCFs can move through porous solids like gases, which is faster than liquid transport through such materials. SCFs have a higher ability to dissolve materials like liquids or solids compared to gases. Near the critical point, small changes in pressure or temperature result in significant changes in density, allowing many properties of an SCF to be fine-tuned. By changing the pressure and temperature, the properties of carbon dioxide can be tuned to be more liquid-like or gas-like.

Fluid properties can be divided into two kinds: equilibrium properties and transport properties. The equation of state can be used accurately to predict the equilibrium properties, such as fluid density, enthalpy, vapour pressure, fugacity and fugacity coefficient, vapour-liquid equilibrium, and all kinds of excess properties.

Supercritical CO_2's thermodynamic properties, such as density or specific heat capacity, vary significantly with slight changes in temperature and pressure due to real gas effects. The Peng-Robinson equation of state (P-R EOS) is used to calculate the thermodynamic properties by accounting for these real gas effects are presented in Appendix A.1.1. The P-R EOS belongs to a specific class of thermodynamic models for modelling the pressure of a solvent as a function of temperature and density and which can be rewritten as a cubic function of the molar volume.

To determine the thermodynamic properties of a real gas, it is necessary to evaluate the departure function of the chosen equation of state for that property. As explained by Elliott [7], the departure function describe the difference between the actual value of a thermodynamic property of a real gas and its value if the gas were ideal under the same temperature and pressure conditions. The ideal gas serves as a reference state to which the properties of real gases are compared. The departure function measures the extent to which a real gas deviates from ideal gas behaviour. The departure functions allow for the accurate calculation of thermodynamic properties for real gases.

The properties of CO_2 are presented as a function of operating conditions (temperature and pressure) in Figure 2. At standard atmospheric pressure and temperature, CO_2 behaves as an ideal gas, and its compressibility factor equals unity. However, at high pressures and/or low temperatures, intermolecular forces between gas molecules become more significant, causing them to deviate from ideal behaviour. As a result, the compressibility factor can be greater than or less than unity, depending on the magnitude of these forces. As presented in Figure 2a, the compressibility factor obtained from the Peng-Robinson equation of state varies strongly depending on the operating conditions.

The real gas effects are also visible on the density plot presented in Figure 2b. The density calculations are based on the compressibility factor, and its value depends on the operating conditions. The fluid properties near the critical point are unique and combine gas-like and liquid-like properties. The details of calculations are explained in Appendix A.1.2.

Figure 2c show the behaviour of the heat capacity of a supercritical fluid at constant pressure (C_p). The details of the calculations can be found in Appendix A.1.3. Contrary to the density, which varies monotonically, the specific heat shows very high levels in a narrow region. In the subcritical region, the phase transition is associated with an effective spike in the heat capacity (i.e., the latent heat). Approaching the critical point, the latent heat falls to zero, which is accompanied by a gradual rise in heat capacity in the pure phases near phase transition. At the critical point, the latent heat

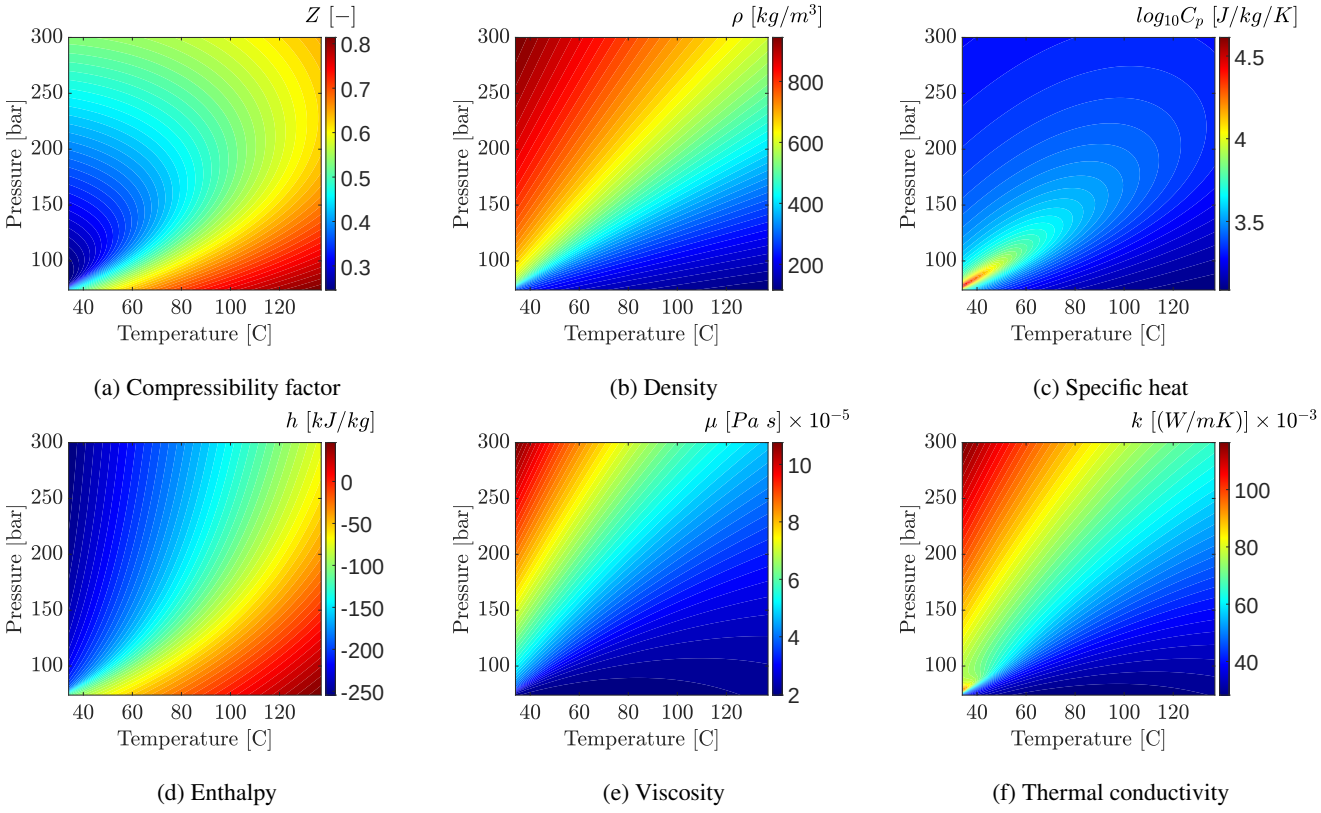

(a) Compressibility factor (b) Density (c) Specific heat

(d) Enthalpy (e) Viscosity (f) Thermal conductivity

Figure 2: Properties of CO_2 based on the equation of state and correlations

is zero, but the heat capacity shows a diverging singularity. Beyond the critical point, there is no divergence, but rather a peak in the heat capacity; the highest point of this peak identifies the Widom line (as discussed by Simeoni et al. [8] and Banuti [9]).

Figure 2d represent how the specific enthalpy change with the operating conditions. The details of calculations are discussed in Appendix A.1.4.

Transport properties, including viscosity and thermal conductivity, are fundamental to the engineering design process for production, fluid transport, and processing operations. However, as Sheng et al. [10] notes, formulating a comprehensive theory for the transport properties of real dense gases and liquids remains a formidable challenge. This difficulty stems from the obstacles in making precise measurements and the complexities of theoretical analysis.

To tackle these challenges, the correlations used to estimate transport coefficients are typically empirical or rooted in theoretical principles. A well-regarded theoretical framework is the Chapman-Enskog theory, as discussed in Chapman and Cowling [11], which addresses the transport properties of dense gases using the distribution function. Originally designed for rigid spherical molecules, the Chapman-Enskog theory requires adaptations to be applicable to real gases. Following this theoretical approach, numerous correlations have been proposed, such as those by Fenghour et al. [12], and Laesecke and Muzny [13] from the National Institute of Standards and Technology (NIST), which utilize reduced density and temperature. The viscosity correlation from Laesecke and Muzny [13] is detailed in Figure 2e.

NIST has formulated a viscosity model that comprises four distinct components: (i) the zero-density limit, (ii) the initial density dependence, (iii) the residual viscosity, and (iv) the critical point viscosity singularity. This NIST viscosity correlation spans temperatures from 100 to 2000 K for gaseous CO_2, and from 220 to 700 K under pressures up to 8000 MPa along the melting line for both compressed and supercritical liquid states. Such correlations and theoretical models are invaluable for accurately predicting the transport properties of real gases and liquids, thereby facilitating engineering design and analytical processes.

Similarly, NIST has formulated a correlation that characterizes the thermal diffusivity behavior of carbon dioxide (CO_2). The study by Huber et al. [14] highlights the unique behavior of thermal conductivity in the vicinity of the critical point. This correlation is valid for temperatures spanning from the triple point to 1100 K and for pressures reaching up to 200 MPa. Figure 2f illustrates the variation in thermal conductivity of carbon dioxide under different operating conditions, demonstrating how it adapts to changes in temperature and pressure.

2.2. Governing equations

The governing equations for quasi-one-dimensional compressible flow in Cartesian coordinates are detailed in

Appendix A.2 and are based on the foundational work by Anderson [15]. Quasi-one-dimensional flow refers to a fluid flow scenario where it's assumed that flow properties are uniformly distributed across any given cross-section. This simplification is typically applied in situations where the flow channel's cross-sectional area changes, such as through irregular shapes or partial fillings of an extractor. In these instances, the flow is considered quasi-one-dimensional because it's presumed that velocity and other flow properties change solely along the flow direction.

The set of quasi-one-dimensional compressible Navier-Stokes equations in Cartesian coordinates are encapsulated by Equations 1 through 3. The formulation of these equations is elaborated upon in Appendix A.2, providing a mathematical foundation for analyzing flow dynamics under the assumed conditions.

$$\frac{\partial\left(\rho_f A_f(z)\right)}{\partial t}+\frac{\partial\left(\rho_f A_f(z) v\right)}{\partial z}=0 \tag{1}$$

$$\frac{\partial\left(\rho_f v A_f(z)\right)}{\partial t}+\frac{\partial\left(\rho_f A_f(z) v^2\right)}{\partial z}=-A_f(z)\frac{\partial P}{\partial z} \tag{2}$$

$$\frac{\partial\left(\rho_f e A_f(z)\right)}{\partial t}+\frac{\partial\left(\rho_f A_f(z) v e\right)}{\partial z}=-P\frac{\left(A_f(z) v\right)}{\partial z}+\frac{\partial}{\partial z}\left(\frac{\partial T}{\partial z}\right) \tag{3}$$

where ρ_f is the density of the fluid, $A_f(z)$ is the function which describe change of the cross-section, v is the velocity, P is the total pressure, e is the internal energy of the fluid, t is time and z is the spacial direction.

Based on governing equations, the small discontinuity (defined as δ) in flow properties, shown in Figure 3, can be analysed. The analysis follows the work of Schreier [16].

	ρ_f	$\rho_f+\delta\rho_f$	
$v\rightarrow$	P	$P+\delta P$	$v+\delta v\rightarrow$
	T	$T+\delta T$	

Figure 3: Small discontinuity in one-dimensional flow

The discontinuity is presumed to be at rest relative, and the balance equations become

$$\rho_f\delta v+v\delta\rho_f+\delta\rho_f\delta v=0$$
$$\delta P=\delta v\delta\rho_f$$

These relations are equally valid if both regions are separated by a region of finite width rather than a discontinuity.

$$\lim_{\rho_f v\rightarrow 0}\rho_f\delta v+v\delta\rho_f+\delta\rho_f\delta v=0/\delta\rho_f\rightarrow\frac{dv}{d\rho_f}=-\frac{v}{\rho_f}$$

By combining the momentum equation with the above equation, we get

$$\frac{dv}{d\rho_f}=-\frac{dv}{dP}\frac{dP}{d\rho_f}=-\frac{1}{\rho v}\frac{dP}{d\rho_f}=-\frac{v}{\rho_f} \tag{4}$$

Suppose the flow is presumed to be isentropic, $dP/d\rho_f = c^2$, so $v^2 = c^2$, where c is the speed of sound. This can be interpreted as a small pressure wave propagating with the speed of sound relative to the flow. Moreover, if the flow velocity is relatively low, all pressure changes are hydrodynamic (due to velocity motion) rather than thermodynamic which leads to $\partial\rho_f/\partial P \approx 0$. In other words, the small changes in pressure due to flow velocity changes do not change the density.

The low Mach number condition leads to the incompressible condition: $\nabla\cdot\mathbf{u}=0$, which is valid for constant density (strict incompressible) or varying density flow. The restraint allows for the removal of acoustic waves, but also allows for large perturbations in density and/or temperature. The assumption is that the flow remains within a Mach number limit (normally less than 0.3) for any solution using such a constraint to be valid. In 1-D case the incompressibility condition becomes $\frac{du}{dz}=0$, so the fluid velocity is constant.

2.3. Extraction model

2.3.1. Continuity equation

The previously derived quasi-one-dimensional continuity equation (Equation 1) is refined by incorporating a function $A_f(z)=A\phi(z)$. This modification accounts for the variability in the cross-sectional area available for fluid flow. Equation 5 presents this adaptation in the differential form of the continuity equation, capturing the dynamics of the flow as it responds to changes in the cross-section.

$$\frac{\partial(\rho_f(T(t,z),P(t))\phi(z))}{\partial t}+\frac{\partial(\rho_f(T(t,z),P(t))vA\phi(z))}{\partial z}=0 \tag{5}$$

where A is the total cross-section of the extractor and $\phi(z)$ describe porosity along the extractor.

Assuming that the mass flow rate is constant in time, the temporal derivative becomes zero, and the spatial derivative can be integrated along z as

$$\int\frac{\partial(\rho_f(T(t,z),P(t))vA\phi(z))}{\partial z}dz=0\rightarrow F=\rho_f(T(t,z),P(t))vA\phi(z) \tag{6}$$

Here, F is a constant obtained from the integration and is understood as the mass flux per unit area, which is assumed to be constant along z. To simplify the dynamics of the system, it is assumed that $F=F(t)$ is a control variable and affects the whole system instantaneously. This assumption allows for finding the velocity profile that satisfies mass continuity based on $F(t)$, $\phi(z)$, and $\rho_f(T(t,z),P(t))$.

$$v=\frac{F(t)}{\rho_f(T(t,z),P(t))A\phi(z)} \tag{7}$$

The fluid density $\rho_f(T(t,z),P(t))$ can be obtained from an equation of state if temperature and the thermodynamic pressure (assumed $P(t)$ to be constant along z due to the low-Mach number condition) are known. The variation in density may be caused by the fluid accumulation in the system (equivalent to pressure change), which occurs instantaneously along z or by a temperature change.

Analogously, the superficial velocity might be introduced to the model and defined as

$$u=v\phi(z)=\frac{F(t)}{\rho_f(T(t,z),P(t))A} \tag{8}$$

2.3.2. Mass balance for the fluid phase

The comprehensive derivation of the mass balance equation for the fluid phase is detailed in Appendix A.2. This equation accounts for the movement of the pseudo-homogeneous fluid phase (Equation 9), which is constrained to the axial direction due to the quasi-one-dimensional approach that considers changes in the void fraction. It is also predicated on the assumption that the thermodynamic pressure remains constant throughout the device, as illustrated by Equation 4. The analysis further simplifies the flow dynamics by disregarding the boundary layer near the extractor's inner wall, leading to a uniform velocity profile across any cross-section perpendicular to the axial direction. Given that the solute concentration in the solvent is negligible, the fluid phase is described as pseudo-homogeneous, with properties identical to the solvent itself. The mass balance equation thus encompasses convection, diffusion, and kinetic terms to accurately represent the fluid phase's behaviour.

$$\frac{\partial c_f(t,z)}{\partial t}+\frac{1}{\phi(z)}\frac{\partial\left(c_f(t,z)u\right)}{\partial z}=\frac{1-\phi(z)}{\phi(z)}r_e(t,z)+\frac{1}{\phi(z)}\frac{\partial}{\partial z}\left(D_e^M\frac{\partial c_f(t,z)}{\partial z}\right) \tag{9}$$

$c_f(t,z)$ represents the concentration of solute in the fluid phase, , $r_e(t,z)$ is a mass transfer kinetic term, and $D_e^M(T(t,z),P(t),F(t))$ is the axial diffusion coefficient.

2.3.3. Mass balance for the solid phase

The solid phase is considered to be stationary, without convection and diffusion terms in the mass balance equation (Equation 10). Therefore, the only significant term in this equation is the kinetic term (as defined in Equation 11), which connects the solid and fluid phases. The extract is represented by a single pseudo-component to simplify the analysis.

$$\frac{\partial c_s(t,z)}{\partial t}=\underbrace{r_e(t,z)}_{\text{Kinetics}} \tag{10}$$

2.3.4. Kinetic term

The kinetic term in this study is based on the two-film theory proposed by Reverchon [6], and the mass transfer kinetic is given by Equation 11. This equation takes into account the overall diffusion coefficient and the concentration gradient, which acts as the driving force for the process.

As the solvent flows through the bed, CO_2 molecules diffuse into the pores and adsorb on the particle surface to form an external fluid film around the solid particles due to the solvent-solid matrix interactions. The effect of Knudsen diffusion is negligible in this process, as the mean free path of the molecule is much smaller than the pore diameter. The dissolved solute diffuses from the particle's core through the solid-fluid interface, the pore, and the film into the bulk. Figure 4 illustrates the mass transfer mechanism, where the mean solute concentration in the solid phase is denoted as c_s and the equilibrium concentrations at the solid-fluid interface are denoted as c_s^* and c_p^*, respectively, for solid and fluid phases. The concentration of the solutes in the fluid phase in the center of the pore is denoted as c_p. As the solute diffuses through the pore, its concentration changes and reaches c_{pf} at the opening of the pore. The solute then diffuses through the film around the particle and reaches bulk concentration c_f. The two-film theory describes the solid-fluid interface inside the pore. The overall mass transfer coefficient can be determined if the relationship between the solute concentration in one phase and its equilibrium concentration is known.

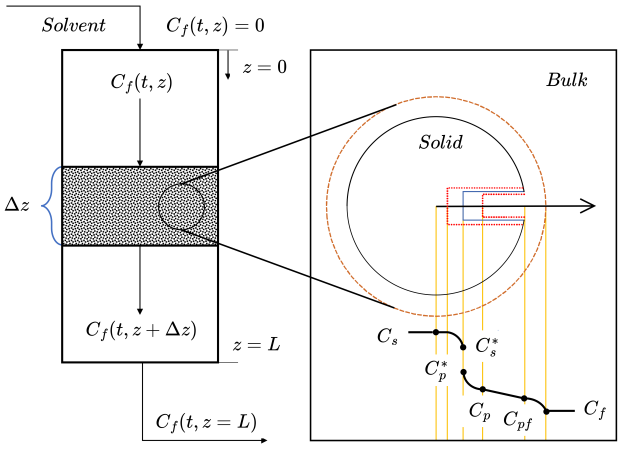

Figure 4: The extraction mechanism

Bulley et al. [17] suggests a process where the driving force for extraction is given by the difference between the concentration of the solute in bulk, c_f, and in the center of the pore, c_p^*. The concentration c_p^* is in equilibrium with c_s according to an equilibrium relationship. The rate of extraction is thus $r_e\left(c_f-c_p^*(c_s)\right)$.

On the other hand, Reverchon [6] proposes a driving force given by the difference between c_s and c_p^*. c_p^* is determined by an equilibrium relationship with c_f and the extraction rate is $r_e\left(c_s-c_p^*(c_f)\right)$ or more precisely

$$r_e(t,z)=\frac{D_i(T(t,z),P(t))}{\mu l^2}\left(c_s(t,z)-c_P^*(t,z)\right) \tag{11}$$

where μ is sphericity, l a characteristic dimension of particles and can be defined as $l=r/3$, r is the mean particle radius, ρ_s is the solid density, $D_i(T(t,z))$ corresponds to the overall diffusion coefficient and $c_P^*(t,z)$ is a concentration at the solid-fluid interface (which according to the internal resistance model is supposed to be at equilibrium with the fluid phase).

According to Bulley et al. [17], a linear equilibrium relationship (equation 12) can be used to find an equilibrium concentration of the solute in the fluid phase $c_f^*(t,z)$ is based on the concentration of the solute in the solid phase $c_s(t,z)$

$$c(t,z)=k_p(T(t,z),P(t))q^*(t,z) \tag{12}$$

The volumetric partition coefficient $k_p(T(t,z),P(t))$ behaves as an equilibrium constant between the solute concentration in one phase and the corresponding equilibrium

concentration at the solid-fluid interphase. According to Spiro and Kandiah [18], the term $k_p(T(t,z),P(t))$ can be expressed as the function of mass partition factor $k_m(T(t,z))$.

$$k_m(T(t,z)) = \frac{k_p(T(t,z),P(t))\rho_s}{\rho(T(t,z),P(t))} \tag{13}$$

Equation 14 represents of the kinetic term according to Reverchon [6]

$$r_e(t,z) = -\frac{D_i(T(t,z),P(t))}{\mu l^2}\left(c_s(t,z) - \frac{\rho_s}{k_m(T(t,z))\rho_f(T(t,z),P(t))}c_f(t,z)\right) \tag{14}$$

2.3.5. *Uneven distribution of the solute in the solid phase*

Following the idea of the Broken-and-Intact Cell (BIC) model presented by Sovova [19], the internal diffusion coefficient D_i is consider to be a product of the reference value of D_i^R and the exponential decay function γ, as given by Equation 15.

$$D_i = D_i^R\gamma(c_s(t,z)) = D_i^R\exp\left(\Upsilon\left(1-\frac{c_s(t,z)}{c_{s0}}\right)\right) \tag{15}$$

where the Υ describe the curvature of the decay function. The final form of the extraction kinetic Equation is given by Equation 16.

$$r_e(t,z) = -\frac{D_i^R(T(t,z),P(t))\gamma(c_s(t,z))}{\mu l^2}\left(c_s(t,z) - \frac{\rho_s}{k_m(T(t,z))\rho(T(t,z),P(t))}c_f(t,z)\right) \tag{16}$$

Such a formulation limits the availability of the solute in the solid phase. Similarly to the BIC model, if solute is assumed to be contained in the cells, a part of which is open because the cell walls were broken by grinding, and the rest remains intact. The diffusion of the solute from a particle's core takes more time compared to the diffusion of the solute located close to the outer surface. Considering that the internal diffusion coefficient decay as the concentration of the solute in the solid decrease. As the value of the c_s decrease over time, the exponential term approach unity and $\lim_{c_s\to 0} D_i = D_i^R$. D_i^R can be interpreted as the internal diffusion coefficient at vanishing gradient.

Alternatively, the decay function γ can be consider with respect to the Shrinking Core model presented by Goto et al. [20], where the particle radius change as the amount of solute in the solid phase decrease. As the particle size decrease due to dissolution, the diffusion path increase which makes the diffusion slower and reduce the value of a diffusion coefficient. The same analogy can be apply to the Equation 15 to explain the change of the diffusion coefficient.

2.3.6. *Heat balance*

The heat governing equation describe the evolution of the energy in the system and it is given by 17. The derivation of the heat equation can be found in Appendix A.2.

$$\frac{\partial\left(\rho_f(T(t,z),P(t))e(t,z)A_f\right)}{\partial t} + \frac{\partial\left(\rho_f(T(t,z),P(t))A_f v e(t,z)\right)}{\partial z}$$
$$= -P(t)\frac{\left(A_f v\right)}{\partial z} + \frac{\partial}{\partial z}\left(\frac{\partial T(t,z)}{\partial z}\right) \tag{17}$$

The departure function is a mathematical function that characterizes the deviation of a thermodynamic property (enthalpy, entropy, and internal energy) of a real substance from that of an ideal gas at the same temperature and pressure. The departure function is typically defined as the difference between the value of a thermodynamic property for a real fluid and the corresponding value for an ideal gas at the same temperature and pressure. They are typically computed by integrating a function that depends on the equation of state and its derivatives. Following Elliott [7] or Gmehling et al. [21], a real gas internal energy definition can be obtained from the departure functions, defined through Equation 18. More information on the departure functions can be found in Appendix A.1.4.

$$de(t,z) = C_v dT - \left[P(t) - T(t,z)\left(\frac{\partial P(t)}{\partial T(t,z)}\right)_{v_m(T(t,z),P(t))}\right]dv_m(T(t,z),P(t)) \tag{18}$$

where $e^{id}(t,z)$ is the internal energy of perfect gas.

Suppose a gas is considered to be perfectly caloric ($e(t,z) = C_v T(t,z)$), then the energy equation can be written explicitly in the form of temperature. The perfectly caloric gas can be seen as the special case of a real gas, where the second term of Equation 18 goes to zero and the heat capacity C_v is constant.

For real gases, it is complicated to write the heat balance in terms of temperature, but it can be used directly in the form of internal energy, as it is given by Equation 3. In such a case, the temperature needs to be recovered from the internal energy. A relation for the internal energy can be obtained from an equation of state. For Peng-Robinson, such a relation is given by Equation 19 as presented by Elliott [7].

$$\frac{e(t,z)-e^{id}(t,z)}{RT(t,z)} = -\frac{A(T(t,z),P(t))}{B(T(t,z),P(t))\sqrt{8}}\frac{\kappa\sqrt{T_r}}{\sqrt{\alpha}}\ln\left[\frac{Z(T(t,z),P(t)) + \left(1+\sqrt{2}\right)B(T(t,z),P(t))}{Z(T(t,z),P(t)) + \left(1-\sqrt{2}\right)B(T(t,z),P(t))}\right] \tag{19}$$

To solve Equation 19, temperature, pressure, and density values need to be known. If an equation of state is introduced, then only two out of three variables need to be obtained as the third one can be calculated; this can be represented as follow

$$e(t,z) = e(T(t,z),P(t),\rho_f(T(t,z),P(t))) = e(T(t,z),P(t),\rho_f(T(t,z),P(t))) \tag{20}$$

If the value of internal energy $e(t,z)$ is known from the time evolution of the energy Equation 3, and pressure is known from measurement, then the temperature can be reconstructed. A roootfinder can be used to find a value of temperature, which minimizes the difference between the value of internal energy coming from the time evolution (Equation 17) and the output from Equation 19. Such a

procedure allows to find a local temperature along spatial direction z and needs to be repeated every time-step.

Another way to express the energy equation is to introduce enthalpy $h(t,z) = e(t,z) + P(t)/\rho_f(T(t,z),P(t))$. By introducing the definition of enthalpy, the energy equation becomes

$$\frac{\partial\left(\rho_f(T(t,z),P(t))h(t,z)A_f\right)}{\partial t} = -\frac{\partial\left(\rho_f(T(t,z),P(t))h(t,z)A_f v\right)}{\partial z} + \frac{\partial\left(P(t)A_f\right)}{\partial t} + \frac{\partial}{\partial z}\left(k\frac{\partial T(t,z)}{\partial z}\right) \tag{21}$$

The main advantage of this formulation is the presence of term $\partial P(t)/\partial t$, which allows it to directly affect the system through the change of thermodynamic pressure (which is a control variable). The enthalpy is related to the pressure and temperature through the following equation:

$$h(t,z) = h(T(t,z),P(t),\rho_f(T(t,z),P(t))) = h(T(t,z),P(t),\rho_f(T(t,z),P(t))) \tag{22}$$

If the value of enthalpy is known from the time evolution and pressure can be measured, then the Equation 22 can be solved for the temperature to recover the temperature profile. For the Peng-Robinson EoS, the enthalpy can be defined by Equation 23. More details can be found in Appendix A.1.4 or given by Gmehling et al. [21].

$$h(t,z) - h(t,z)^{id} = RT(t,z)\left[T_r(Z(T(t,z),P(t)) - 1) - 2.078(1+\kappa)\sqrt{\alpha(T(t,z))}\ln\left(\frac{Z(T(t,z),P(t)) + \left(1+\sqrt{2}\right)B(T(t,z),P(t))}{Z(T(t,z),P(t)) + \left(1-\sqrt{2}\right)B(T(t,z),P(t))}\right)\right] \tag{23}$$

The Equation 23 requires an reference sate, which in this case is assumed to be $T_{ref} = 298.15\ [K]$ and $P_{ref} = 1.01325\ [bar]$.

As discussed by Gmehling et al. [21], the influence of the intermolecular forces on the enthalpy is needs to taken into account in high pressures systems. In most cases, these forces are attractive, so additional energy is necessary to move the molecules away from each other, that is, to lower the density. If this energy is not added, the substance cools down when it is expanded.

2.3.7. Pressure term

The pressure term in the energy equation, given by Equation 21, describes the change of the thermodynamic pressure with respect to time. As explained in Chapters 2.2, at Low-Mach number conditions, the thermodynamic pressure is nearly constant in space due to the small pressure wave propagation that occurs at the speed of sound. Under such conditions, the term $\partial P/\partial t$ can be approximated by an ordinary differential equation, which describes the instantaneous change of pressure in the system. The pressure (P) in the system is considered a state variable, while the pressure in the new time-step (P_{in}) is considered a control variable.

$$\frac{\partial P(t)}{\partial t} \approx \frac{P(t) - P_{in}(t)}{\Delta t} \tag{24}$$

Such a simplified equation takes into account the pressure change in the energy balance, but the dynamics are simplified and do not consider the effects of pressure losses. In a real system, the dynamics of pressure change would depend on a pump used in an extraction system, as well as a back-pressure regulator used to control an outlet valve.

2.3.8. Extraction yield

The efficiency of the process (the yield) is calculated according to Equation 25 as presented by Sovova et al. [22]. The measurement equation evaluate the mass of solute at the outlet of the extraction unit and sums it. The integral form of the measurement equation (25) can be transformed into the differential form (26) and augmented with the process model.

$$y(t) = \int_{t_0}^{t_f} \frac{F(t)}{\rho_f(T(t,z),P(t))} c_f(t,z)\Big|_{z=L} dt \tag{25}$$

$$\frac{dy(t)}{dt} = \frac{F(t)}{\rho_f(T(t,z),P(t))} c_f(t,z)\Big|_{z=L} \tag{26}$$

2.3.9. Initial and boundary conditions

It is assumed that the solvent is free of solute at the entrance of the extractor and that all the solid particles have the same initial solute content c_{s0}. As the residence time is much shorter than the sampling time, the initial state estimate for the concentration of the solute in the fluid phase would be not reliable. Considering that it is assumed that the $c_{f0} = 0$. Moreover, it is considered that the initial temperature of the extractor in every place is the same and described by h_0. Therefore, the initial conditions employed in the simulation are:

$$c_f(t=0,z) = 0 \qquad c_s(t=0,z) = c_{s0} \qquad h(t=0,z) = h_0$$
$$\frac{\partial c_f(t,z=L)}{\partial x} = 0 \qquad c_s(t=0,z) = c_{s0} \qquad \frac{\partial h(t,z=L)}{\partial x} = 0$$

2.3.10. State-space representation

The process model can be written in a general form:

$$\begin{bmatrix} \frac{\partial c_f(t,z)}{\partial t} \\ \frac{\partial c_s(t,z)}{\partial t} \\ \frac{\partial h(t,z)}{\partial t} \\ \frac{\partial P(t,z)}{\partial t} \\ \frac{\partial y(t)}{\partial t} \end{bmatrix} = \begin{bmatrix} \bar{\phi}_1\left(c_f(t,z),c_s(t,z),h(t,z);\Theta\right) \\ \bar{\phi}_2\left(c_f(t,z),c_s(t,z),h(t,z);\Theta\right) \\ \bar{\phi}_3\left(c_f(t,z),c_s(t,z),h(t,z);\Theta\right) \\ \bar{\phi}_4\left(c_f(t,z),c_s(t,z),h(t,z);\Theta\right) \\ \bar{\phi}_5\left(c_f(t,z),c_s(t,z),h(t,z);\Theta\right) \end{bmatrix} = \bar{\phi}\left(t,z;\Theta\right) = \frac{\partial \chi(t,z)}{\partial t} \tag{27}$$

where Θ is a paramter space, $\bar{\phi}$ is a set of functions that correspond to state equations of the model, and χ is the state-space model.

Function $\bar{\phi}$ are transformed to a corresponding set of N_z discretized equations denoted as G. The state-space model $\chi(t,z)$ after the discretization is represented by $\dot{x}(t)$.

$$\dot{x}(t) = \frac{dx(t)}{dt} = \begin{bmatrix} \frac{dc_{f,1}(t)}{dt} \\ \vdots \\ \frac{dc_{f,N_z}(t)}{dt} \\ \hline \frac{dc_{s,1}(t)}{dt} \\ \vdots \\ \frac{dc_{s,N_z}(t)}{dt} \\ \hline \frac{dh_1(t)}{dt} \\ \vdots \\ \frac{dh_{N_z}(t)}{dt} \\ \hline \frac{dP(t)}{dt} \\ \hline \frac{dy(t)}{dt} \end{bmatrix} = \underbrace{\begin{bmatrix} G_1\left(c_f(t), c_s(t), h(t); \Theta\right) \\ \vdots \\ G_{N_z}\left(c_f(t), c_s(t), h(t); \Theta\right) \\ \hline G_{N_z+1}\left(c_f(t), c_s(t), h(t); \Theta\right) \\ \vdots \\ G_{2N_z}\left(c(t), c_s(t), h(t); \Theta\right) \\ \hline G_{2N_z+1}\left(c_f(t), c_s(t), h(t); \Theta\right) \\ \vdots \\ G_{3N_z}\left(c_f(t), c_s(t), h(t); \Theta\right) \\ \hline G_{3N_z+1}\left(c_f(t), c_s(t), h(t); \Theta\right) \\ \hline G_{3N_z+2}\left(c_f(t), c_s(t), h(t); \Theta\right) \end{bmatrix}}_{G(x(t);\Theta)}$$

where $x \in \mathbb{R}^{N_x=3N_z}$ and $\Theta \in \mathbb{R}^{N_\Theta=N_\theta+N_u}$, N_θ is the number of model parameters, N_u is the number of control variables.

In a state-space sense, the state variables of the system are the local concentrations of solute in the fluid and solid phases ($c_f(t,z)$ and $c_s(t,z)$, respectively), and the local enthalpy of the pseudo-homogeneous phase ($h(t,z)$). The controllable input variables are the mass flow rate and temperature of the solvent in the feed and the pressure in the extractor. Additionally, the pressure change is augmented with the state-space and denoted as $P(t)$. The system state-space is extended by assuming that extraction yield can be modelled as a function of a known initial mass of solute in the solid phase, and it can be measured after the separator ($Y(t)$). The system is controllable by manipulating the flow rate and temperature (enthalpy) of CO_2 in the feed and the pressure in the extractor.

2.3.11. Discretization methods

The method of lines is used to transform the process model equations into a set of ODEs denoted as $G(x(t);\Theta)$. The partial derivatives in z-direction are computed using a first-order and second-order finite difference approximation. The backward finite difference is used to approximate the first-order derivative, while the central difference scheme is used to approximate the second-order derivative. The length of the fixed bed is divided into N_z equally distributed points in z-direction.

As presented in Appendix A.2, all the governing can be written in the integral form using the Divergence Theorem. The integral equation states that the change rate of the integral of any quantity over an arbitrary control volume is given by the flux through the boundary of the control volume, with being the outer surface normal through the boundary. That quantity is neither produced nor consumed inside the control volume and is conserved. For a derivative to be conservative, it must form a telescoping series. In other words, after the addition of all terms coming from the discretization over a grid, only the boundary terms should remain, and the artificial interior points should cancel out. To ensure mass conservation, discretization is applied to the conservative form of the process model.

2.4. Parameter estimation

Only some of the parameters in a process model can be estimated from the theoretical considerations. The goal of parameter estimation is to obtain the "best" estimate of unknown parameters θ (which is a subset of the parameter space Θ containing all parameters of a model) based on the continuous observations $Y(t)$ or the discrete observations $Y(t_i)$. Conceptually, the unobservable error $\epsilon(t)$ is added to the deterministic model output, $y(t)$ (Equation 25), to give the observable dependent variable $Y(t)$ (for example results of an experiment). For discrete observations, this can be expressed as:

$$Y(t_i) = y(\theta, t_i) + \epsilon(t_i)$$

For continuous variables, the equation is:

$$Y(t) = y(\theta, t) + \epsilon(t)$$

However, obtaining analytical solutions for a deterministic process model can be challenging, so experiments are often conducted where the vector of derivatives $dY(t_i)/dt$ is measured instead of $Y(t_i)$ itself. In such cases, it is assumed that the unobservable error is added to the deterministic derivative $dy(\theta, t_i)/dt$ as shown below

$$\frac{dY(t_i)}{dt} = \frac{dy(\theta, t_i)}{dt} + \epsilon(t_i) \tag{28}$$

In the case where the error in the first observation is denoted as ϵ_1, the error in the second observation ϵ_2' incorporates ϵ_1 as well as an independent random component, given by $\epsilon_2' = \epsilon_1 + \epsilon_2$. Similarly, the error in the third observation is $\epsilon_3' = \epsilon_1 + \epsilon_2 + \epsilon_3$, etc. Mandel [23] made a distinction between the typically assumed independent measurement error in the dependent variable and a "cumulative" or interval error, in which each new observation encompasses the error of the previous ones. Cumulative errors arise from fluctuations in the process due to small variations in operating conditions and are not independent; only the differences in measurement from one period to the next are independent.

Maximum likelihood estimation (MLE) is a statistical method used to estimate the parameters of a probability distribution based on observed data. The MLE works by finding the values of the parameters that maximize the likelihood function, which is the probability of observing the given data for a given set of parameter values. The MLE has desirable properties such as asymptotic efficiency and normality. Although the MLE has often been associated with the normal distribution for mathematical convenience, it can be applied to a wide range of probability distributions. The derivation of the likelihood function under the assumption of the Gaussian distribution is presented in Appendix A.4. The

final form of the objective function is presented by Equation 29:

$$\ln L = -\frac{n}{2}\ln\left(2\pi\sigma^2\right) - \frac{\sum_{i=1}^{n}\left[\frac{dY(t_i)}{dt} - \frac{dy(\theta,t_i)}{dt}\right]^2}{2\sigma^2} \tag{29}$$

The parameter estimation problem can be formulated as follow:

$$\begin{aligned} \hat{\theta}_{MLE} &= \arg\max_{\sigma,\theta\in\Theta} \ln L = \arg\max_{\sigma,\theta\in\Theta} p(\theta|y) \\ \text{subject to} \quad \dot{x} &= G(x(t);\theta) \\ \dot{\theta} &= 0 \\ y &= y(t) \\ \theta^{lb} &\le \theta \le \theta^{ub} \end{aligned} \tag{30}$$

where $\hat{\theta}$ is as maximum likelihood estimator, θ^{lb} define the minimal value of θ, θ^{ub} is the maximum value of θ and σ represents the standard deviation of the residuals (errors) between the observed data points and the model outputs.

The initial guess for each decision variable, as well as the lower and upper bounds are given in Table 1.

Parameter	k_m[-]	$D_i^R \times 10^{-13}[m^2/s]$	$D_e^M \times 10^{-12}[m^2/s]$	Υ [-]
Lower bound	0	0	0	0
Upper bound	$+\infty$	$+\infty$	$+\infty$	$+\infty$
Initial guesses	0.1-10	$0.1-10$	0.1-10	0.1-10

Table 1: Constraints and initial guess

Solution of Equations 30 yield the desired estimates $\hat{\theta}$. For some models, these equations can be explicitly solved for $\hat{\theta}$ but in general, no closed-form solution to the maximization problem is known or available, and a maximum likelihood estimator can only be found via numerical optimization.

2.5. Experimental work

In order to solve the optimization problem presented by Equation 30, it is necessary to have knowledge of the dataset $Y(t)$, which was obtained by extracting oil from chamomile flowers. The experiments were performed by Povh et al. [24]. To prepare the flowers for extraction, they were first pre-treated using a knife mill (TECNAL, model TE 340) to reduce their particle size. The mean particle diameter was determined by the Sauter equation and is equal to 0.3×10^{-3}m. The actual density of the chamomile particles was measured through helium pycnometry at the Institute of Chemistry IQ/Unicamp's Analytical Facilities. The bulk density of the bed was computed based on the feed's mass and the extractor's volume. The total porosity of the bed, including the particles, was determined using the following calculation: $\epsilon = 1 - \frac{d_a}{d_r} = 1 - \frac{370}{1364} = 0.73$.

The experiments were conducted using an extractor with diameter of 3.96×10^{-2} m and length 16.55×10^{-2} m. Twelve experiments were performed under different but constant in time operating conditions: $30-40°C$, $100-200$ bar, and $1.33-6.67\times10^{-5}$ kg/s. The amount of solid material used for extraction was 75×10^{-3} kg, which was sufficient to fill the whole vessel. Samples were collected every 30 min for the first 3 h and every hour afterwards up to 10 h.

3. Results

To solve the parameter estimation problem, the single shooting method was used to transform the boundary-value problem into the initial value problem and to formulate the non-linear programming problem. This non-linear optimization task was tackled using the CasADi framework (Andersson et al. [25]). Each time series was fitted separately to the model with the linear extraction kinetics (Equation 14). The initial value problem was solved multiple times with varying initial guesses to identify the global minimum. Within the model context characterized by linear kinetics, two parameters remain to be determined: the partition coefficient k_m and the internal diffusion coefficient D_i.

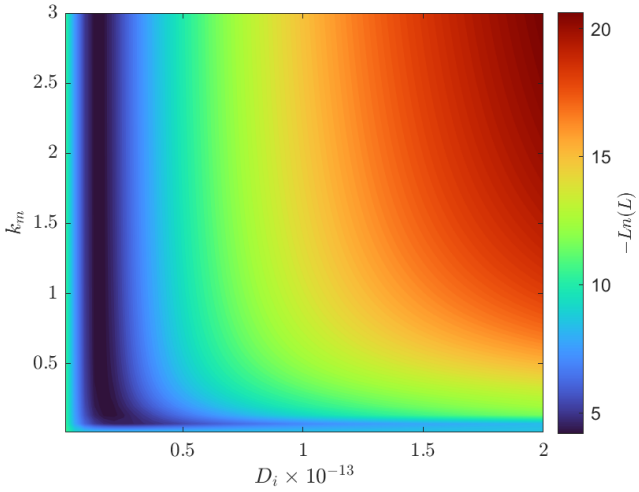

Figure 5: Parameter space for the linear extraction kinetic model and the experiment 1

Figure 5 shows the parameter space and corresponding values of the cost function for experiment 1 ($40°C$, 100 bar and 6.67×10^{-5} kg/s). As the cost function is to be minimized, the lowest value of $-\ln(L)$ indicate the best fit. A black vertical stripe at $D_i \approx 0.2$ can be observed. That stripe indicates the existence of the optimal value of the D_i. In the direction of k_m, the cost function is almost flat, which suggests that any value of k_m above 0.1 fits the data equally well. If k_m can be an arbitrary point, then it can grow to infinity, which suggests that the solvent is far from the saturation, and the model can be simplified. The model reduction can be introduced by considering the limit of k_m in the extraction kinetic term:

$$\lim_{k_m\to\infty}\left(c_s(t,z) - \frac{\rho_s}{k_m(T(t,z))\rho(T(t,z),P(t))}c_f(t,z)\right) =$$
$$= \left(c_s(t,z) - \frac{\rho_s}{\infty\cdot\rho(T(t,z),P(t))}c_f(t,z)\right) = \left(c_s(t,z) - 0\right)$$

The extraction model can be adapted to incorporate adjustments for the reduced kinetic term and axial diffusion. In this revised setup, two parameters remain undetermined: the internal diffusion coefficient D_i and the axial diffusion coefficient D_e^M. Figure 6 illustrates the parameter space and associated cost function values.

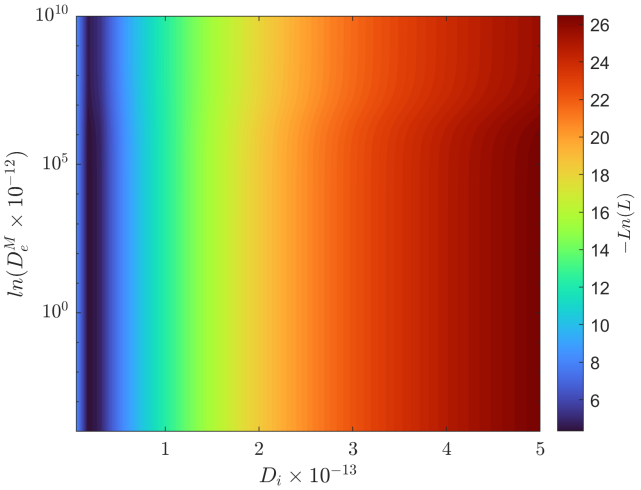

Figure 6: Parameter space for the reduced linear extraction kinetic model with and the experiment 1

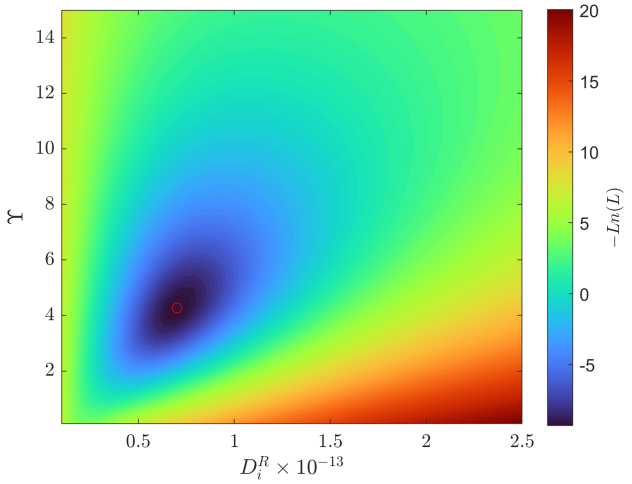

Figure 7: Parameter space for the modified extraction model and experiment 1

Similarly to the previous case, the optimal value of D_i exists, but a unique value for the D_e^M cannot be determined. Figure 6 illustrates the minimal impact of the axial diffusion coefficient, where a broad range of D_e^M yields identical cost function values. By selecting a low value D_e^M, the axial diffusion terms can be reduced or eliminated from the model without compromising its generality. This observation aligns with the findings of Rahimi et al. [26], who analysed the same dataset and reported Peclet numbers ranging between 290 and 400. Such high values of the Peclet number suggest that the advection term dominates the mass transfer, and the axial diffusion is negligible.

In both scenarios previously discussed, the fitting outcomes were not deemed satisfactory. Building upon the concepts underlying the Broken-and-Intact and Shrinking Core models (detailed in Chapter 2.3.5), a gamma function is introduced to capture the diminishing extraction kinetics. The correction factor is combined with the simplified linear model, resulting in a two-parameter model (D_i^R and Υ) as given by Equation 16. Figure 7 shows the parameter space and the corresponding cost function values.

The parameter space for the revised model exhibits a distinct minimum value corresponding to the solution of the parameter estimation problem for experiment 1. The red circle highlights the minimum value of the cost function found by the optimizer. The remaining experiments are fitted to the modified extraction model, and results are presented in Figure 8. The obtained results show good agreement with experimental data.

The estimated parameters describe the diminishing trend of the internal diffusion coefficient D_i, as delineated by Equation 15. It is hypothesized that the internal diffusion coefficient decreases because solute particles face greater difficulty diffusing from the core of a particle than from positions closer to the surface. Decay patterns under various operational conditions, depicted in Figure 9, show that the internal diffusion coefficient is notably higher in

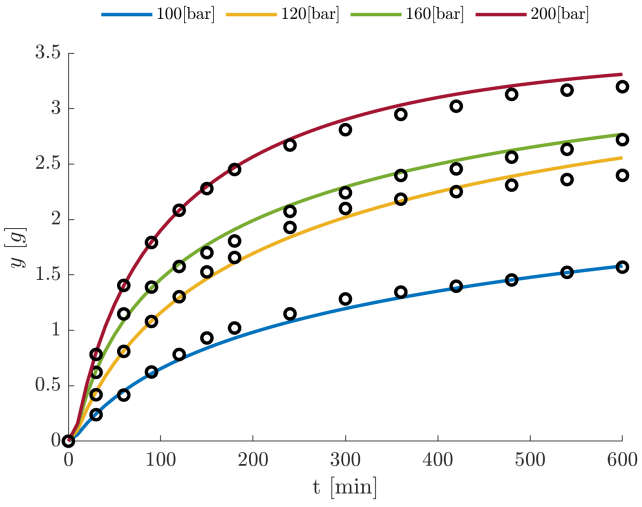

(a) Results of parameter estimation for experiments at 6.67×10^{-5} [kg/s] and temperature of 40 [°C]

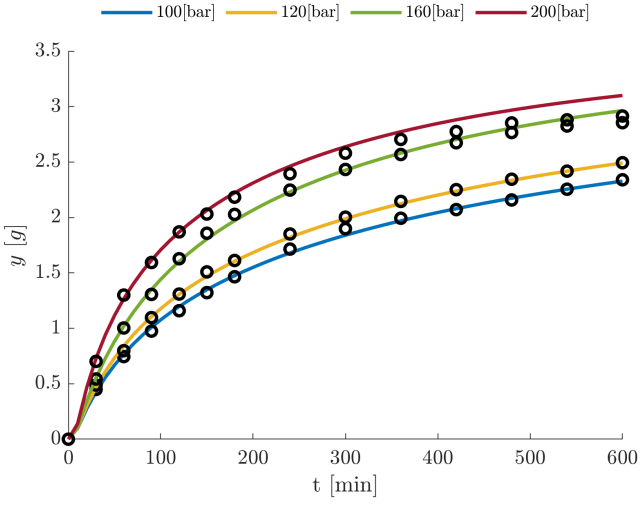

(b) Results of parameter estimation for experiments at 6.67×10^{-5} [kg/s] and temperature of 30 [°C]

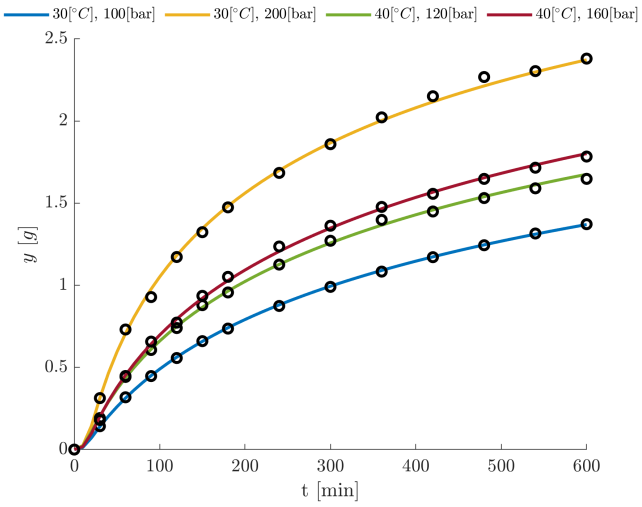

(c) Results of parameter estimation for experiments at 3.33×10^{-5} [kg/s]

Figure 8: Parameter estimation results

fluids under high pressure. This observation aligns with the findings of Giddings et al. [27], Gurdial et al. [28], and Machida et al. [29], who explored the solvation capability of solvents and its correlation with the physical properties of CO_2 by calculating the Hildebrand solubility parameter δ_H. Giddings et al. [27] introduced a correlation for the solubility parameter $\delta_H[\mathrm{MPa}^{1/2}] = 1.25 P_c^{1/2} \rho_r$, with P_c and ρ_r representing the critical pressure and reduced density, respectively. Similarly, Marcus [30] formulated a correlation based on the Van der Waals equation of state: $\delta_H[\mathrm{MPa}^{1/2}] = 2.79 P_c^{1/4} T_r^{1/4} \rho_r$. As Figure 9 shows, fluids with higher solubility factors exhibit greater internal diffusion coefficients. However, the relationship between δ_H and D_i should be considered indicative rather than definitive due to the non-ideal nature of the system and the omission of external factors such as fluid velocity.

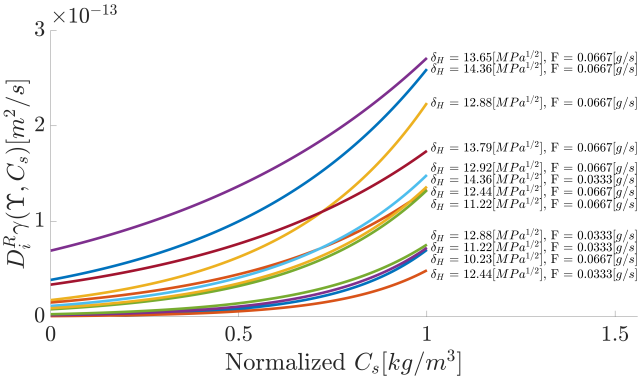

Figure 9: The decaying internal diffusion coefficient

The parameter estimation results are combined to analyse the relationship between the obtained parameters and the operating conditions. Unlike traditional methods that employ a combination of Reynolds, Schmidt, and Sherwood numbers to find correlations—omitted here due to the insignificance of axial diffusion—the approach in this study leverages the Reynolds number $\left(Re = \frac{(2r) \cdot \rho_f \cdot u}{\mu} \right)$ as the sole independent variable. Using the Reynolds number has the advantage of considering the influence of all the control variables (temperature, pressure and flow rate), which means it can be uniquely defined by selecting operating conditions.

In Figures 10a and 10b, two distinct data clusters emerge, each corresponding to a different mass flow rate. Despite the linear trends observed in both sets of correlations, the correlations for D_i^R exhibit a decline with increasing Re, whereas those for Υ show an upward trend with Re. The decrease in D_i^R across each data line can be attributed to higher fluid density and increased mass transfer resistance. Conversely, the rise in Υ correlations may be explained by enhanced solubility. The Hildebrand solubility factor and the Reynolds number are proportional to the fluid density; hence, Υ can be correlated with Re.

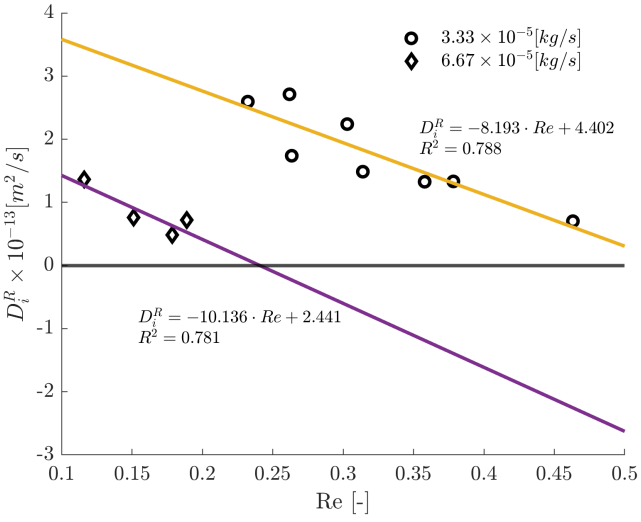

(a) Linear regression $D_i^R = f(Re)$

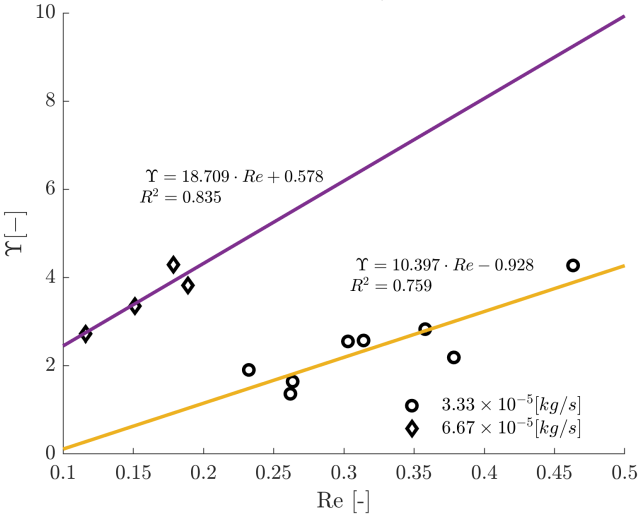

(b) Linear regression $\Upsilon = f(Re)$

Figure 10: Parameter estimation results

A more general relationship can be obtained by applying multiple linear regression instead of linear regression. The clusters in Figure 10 are close to parallel, suggesting that a plane would combine all the data points. The Reynolds number and flow rate act as independent variables for D_i^R and Υ as presented in Figure 11.

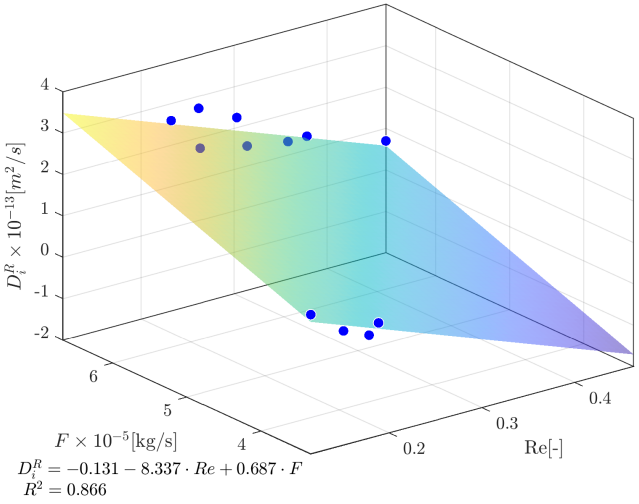

(a) Multiple linear regression $D_i^R = f(Re, F)$

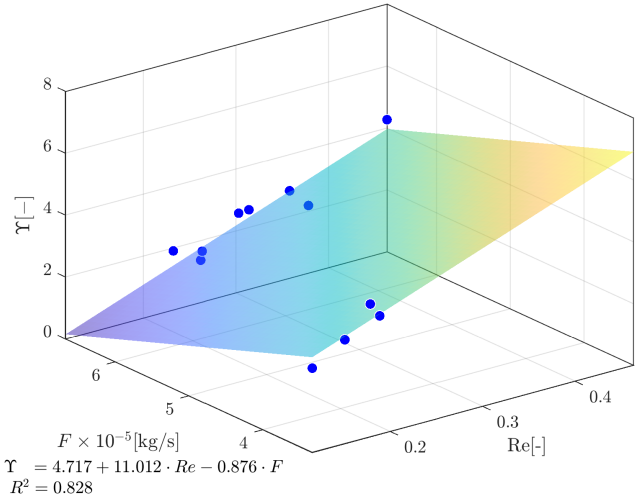

(b) Multiple linear regression $\Upsilon = f(Re, F)$

Figure 11: Parameter estimation results

4. Conclusions

The article presents a comprehensive study on supercritical fluid extraction of essential oil from chamomile flowers, focusing on developing and applying a distributed-parameter model to describe the fluid-solid extraction process. By employing the concept of quasi-one-dimensional flow, the study simplifies the spatial dimensions of the extraction process, ensuring uniform flow across any cross-section while allowing for variations in the area available for the fluid phase. The physical properties of the solvent are estimated using the Peng-Robinson equation of state, and key model parameters are determined through maximum likelihood estimation based on experimental data, considering normally distributed errors.

Laboratory experiments were conducted under various conditions to validate the model. The model parameters, such as partition factor, internal diffusion coefficient, axial diffusion coefficient, and decaying factor, were determined through maximum likelihood estimation based on experimental data. The parameter space exploration revealed that while some parameters could be determined with a high degree of confidence, others, like the axial diffusion coefficient, had a low impact on the model's output. The identification of the low impact parameters lead to model reduction

The Reynolds number and Hildebrand solubility parameter were used to analyse the obtained parameters further. The linear correlations between parameters and the Reynolds numbers are presented. D_i^R coefficient decreases with the Reynolds number due to higher fluids density and the corresponding mass transfer resistance, while Υ increases due to increased Hildebrand parameter. It should be noted that outside of the confidence region, the parameters can become negative, which might reverse the direction of the mass transfer and leads to unfeasible solution.

The presented model can be further used with presented correlations to introduce an extraction model with dynamically changing operating conditions for multiple purposes such as yield maximisation, techno-economic analysis, or optimal design of experiments.

References

[1] Ompal Singh, Zakia Khanam, Neelam Misra, and ManojKumar Srivastava. Chamomile (matricaria chamomilla l.): An overview. Pharmacognosy Reviews, 5(9):82, 2011. ISSN 0973-7847. doi: 10.4103/0973-7847.79103.

[2] Janmejai Srivastava. Extraction, characterization, stability and biological activity of flavonoids isolated from chamomile flowers. Molecular and Cellular Pharmacology, 1(3):138–147, August 2009. ISSN 1938-1247. doi: 10.4255/mcpharmacol.09.18.

[3] Anne Orav, Ain Raal, and Elmar Arak. Content and composition of the essential oil ofchamomilla recutita(l.) rauschert from some european countries. Natural Product Research, 24(1):48–55, January 2010. ISSN 1478-6427. doi: 10.1080/14786410802560690.

[4] Ernesto Reverchon, Giorgio Donsi, and Libero Sesti Osseo. Modeling of supercritical fluid extraction from herbaceous matrices. Industrial & Engineering Chemistry Research, 32(11):2721–2726, nov 1993. doi: 10.1021/ie00023a039.

[5] H. Sovova. Rate of the vegetable oil extraction with supercritical co2. modelling of extraction curves. Chemical Engineering Science, 49 (3):409–414, 1994. doi: 10.1016/0009-2509(94)87012-8.

[6] E. Reverchon. Mathematical modeling of supercritical extraction of sage oil. AIChE Journal, 42(6):1765–1771, jun 1996. doi: 10.1002/aic.690420627.

[7] J Elliott. Introductory chemical engineering thermodynamics. Prentice Hall, Upper Saddle River, NJ, 2011. ISBN 9780136068549.

[8] G. G. Simeoni, T. Bryk, F. A. Gorelli, M. Krisch, G. Ruocco, M. Santoro, and T. Scopigno. The widom line as the crossover between liquid-like and gas-like behaviour in supercritical fluids. Nature Physics, 6(7):503–507, jun 2010. doi: 10.1038/nphys1683.

[9] Daniel Banuti. The latent heat of supercritical fluids. Periodica Polytechnica Chemical Engineering, 63(2):270–275, jan 2019. doi: 10.3311/ppch.12871.

[10] W. Sheng, G. J. Chen, and H. C. Lu. Prediction of transport properties of dense gases and liquids by the peng-robinson (PR) equation of state. International Journal of Thermophysics, 10(1):133–144, jan 1989. doi: 10.1007/bf00500714.

[11] Sydney Chapman and T. G. Cowling. The Mathematical Theory of Non-uniform Gases. Cambridge University Press, 1991. ISBN 9780521408448.

[12] A. Fenghour, William A. Wakeham, and V. Vesovic. The viscosity of carbon dioxide. Journal of Physical and Chemical Reference Data, 27 (1):31–44, jan 1998. doi: 10.1063/1.556013.

[13] Arno Laesecke and Chris D. Muzny. Reference correlation for the viscosity of carbon dioxide. Journal of Physical and Chemical Reference Data, 46(1):013107, mar 2017. doi: 10.1063/1.4977429.

[14] M. L. Huber, E. A. Sykioti, M. J. Assael, and R. A. Perkins. Reference correlation of the thermal conductivity of carbon dioxide from the triple point to 1100 k and up to 200 MPa. Journal of Physical and Chemical Reference Data, 45(1):013102, mar 2016. doi: 10.1063/1.4940892.

[15] John D. Anderson. Computational fluid dynamics the basic with applications. McGraw-Hill, 1995. ISBN 9780071132107.

[16] Stefan Schreier. Compressible flow. Wiley, 1982. ISBN 047105691X.

[17] N. R. Bulley, M. Fattori, A. Meisen, and L. Moyls. Supercritical fluid extraction of vegetable oil seeds. Journal of the American Oil Chemists' Society, 61(8):1362–1365, aug 1984. doi: 10.1007/bf02542243.

[18] M. Spiro and M. Kandiah. Extraction of ginger rhizome: partition constants and other equilibrium properties in organic solvents and in supercritical carbon dioxide. International Journal of Food Science & Technology, 25(5):566–575, jun 2007. doi: 10.1111/j.1365-2621.1990.tb01116.x.

[19] Helena Sovova. Broken-and-intact cell model for supercritical fluid extraction: Its origin and limits. The Journal of Supercritical Fluids, 129:3–8, nov 2017. doi: 10.1016/j.supflu.2017.02.014.

[20] Motonobu Goto, Bhupesh C. Roy, and Tsutomu Hirose. Shrinking-core leaching model for supercritical-fluid extraction. The Journal of Supercritical Fluids, 9(2):128–133, jun 1996. doi: 10.1016/s0896-8446(96)90009-1.

[21] Jürgen Gmehling, Michael Kleiber, Bärbel Kolbe, and Jürgen Rarey. Chemical Thermodynamics for Process Simulation. Wiley, mar 2019. doi: 10.1002/9783527809479.

[22] H. Sovova, R. Komers, J. Kucuera, and J. Jezu. Supercritical carbon dioxide extraction of caraway essential oil. Chemical Engineering Science, 49(15):2499–2505, aug 1994. doi: 10.1016/0009-2509(94)e0058-x.

[23] John Mandel. Fitting a straight line to certain types of cumulative data. Journal of the American Statistical Association, 52(280):552–566, dec 1957. doi: 10.1080/01621459.1957.10501413.

[24] Nanci P. Povh, Marcia O.M. Marques, and M.Angela A. Meireles. Supercritical co2 extraction of essential oil and oleoresin from chamomile (chamomilla recutita [l.] rauschert). The Journal of Supercritical Fluids, 21(3):245–256, November 2001. ISSN 0896-8446. doi: 10.1016/s0896-8446(01)00096-1.

[25] Joel A. E. Andersson, Joris Gillis, Greg Horn, James B. Rawlings, and Moritz Diehl. CasADi: a software framework for nonlinear optimization and optimal control. Mathematical Programming Computation, 11(1):1–36, jul 2018. doi: 10.1007/s12532-018-0139-4.

[26] E. Rahimi, J.M. Prado, G. Zahedi, and M.A.A. Meireles. Chamomile extraction with supercritical carbon dioxide: Mathematical modeling and optimization. The Journal of Supercritical Fluids, 56(1):80–88, February 2011. ISSN 0896-8446. doi: 10.1016/j.supflu.2010.11.008.

[27] J. Calvin Giddings, Marcus N. Myers, Lilian McLaren, and Roy A. Keller. High pressure gas chromatography of nonvolatile species: Compressed gas is used to cause migration of intractable solutes. Science, 162(3849):67–73, October 1968. ISSN 1095-9203. doi: 10.1126/science.162.3849.67.

[28] G.S. Gurdial, P.A. Wells, N.R. Foster, and R.P. Chaplin. The role of polarity in correlations of solid-supercritical fluid phase systems. The Journal of Supercritical Fluids, 2(2–3):85–96, December 1989. ISSN 0896-8446. doi: 10.1016/0896-8446(89)90015-6.

[29] Hiroshi Machida, Masafumi Takesue, and Richard L. Smith. Green chemical processes with supercritical fluids: Properties, materials, separations and energy. The Journal of Supercritical Fluids, 60:2–15, December 2011. ISSN 0896-8446. doi: 10.1016/j.supflu.2011.04.016.

[30] Yizhak Marcus. Are solubility parameters relevant to supercritical fluids? The Journal of Supercritical Fluids, 38(1):7–12, August 2006. ISSN 0896-8446. doi: 10.1016/j.supflu.2005.11.008.

[31] Ding-Yu Peng and Donald B. Robinson. A new two-constant equation of state. Industrial & Engineering Chemistry Fundamentals, 15(1):59–64, feb 1976. doi: 10.1021/i160057a011.

[32] R. M. Pratt. Thermodynamic properties involving derivatives: Using the peng-robinson equation of state,. Chemical Engineering Education, 35:112–139, 2001. ISSN 0009-2479. URL https://www.tib.eu/de/suchen/id/BLSE%3ARN095457101.

[33] B. G. Kyle. Chemical and process thermodynamics. Prentice Hall PTR, 1999. ISBN 0130874116.

[34] Bruce E. Poling. The properties of gases and liquids. McGraw-Hill, 2001. ISBN 0070116822.

A. Appendix

A.1. Thermodynamic

A.1.1. Equation of state and properties of the fluid phase

A cubic equation of state serves as a mathematical model to describe the behavior of real gases and liquids through a third-degree polynomial equation that correlates the pressure, volume, and temperature of a substance. These equations constitute tools for comprehending the phase behavior, properties, and thermodynamic processes of actual substances, across various engineering and scientific applications. The cubic equation of state take into account deviations from ideal gas behavior, which are particularly important at high pressures and low temperatures, where real gases do not follow assumption of ideal gas.

$$P = \frac{RT}{v_m - b} - \frac{\Phi}{v_m^2 - ubv_m + wb^2} \tag{31}$$

In this equation, P denotes the pressure of the substance, v_m represents the molar volume of the substance, T stands for the absolute temperature of the substance, u and w are integers that vary from one equation to another, R symbolizes the universal gas constant, and a and b serve as substance-specific parameters known as Van der Waals constants. ω denotes an acentric factor and $\Phi = a\alpha$.

The Van der Waals constants, a and b, constitute empirical values contingent upon the particular substance being modeled. These constants factor in molecular interactions (represented by 'a') and the finite size of gas molecules (indicated by 'b').

Several variations of the cubic equation of state exist each with its own set of parameters and assumptions. Tables 2 show parameters for popular cubic EoS.

EoS	u	w	a	b
van der Waals	0	0	$\frac{27}{64}\frac{R^2T_c^2}{P_c}$	$\frac{RT_c}{8P_c}$
Redlich and Kwong	1	0	$0.42748\frac{R^2T_c^{2.5}}{P_c}$	$\frac{0.08664RT_c}{P_c}$
Soave	1	0	$0.42748\frac{R^2T_c^2}{P_c}$	$\frac{0.08664RT_c}{P_c}$
Peng and Robinson [31]	2	-1	$0.45724\frac{R^2T_c^2}{P_c}$	$\frac{0.07780T_c}{P_c}$

Table 2: Parameters for Popular Cubic EoS

EoS	α	f(ω)
van der Waals	-	-
Redlich and Kwong	$\frac{1}{\sqrt{T_r}}$	-
Soave	$\left[1 + f(\omega)\left(1 - \sqrt{T_r}\right)\right]^2$	0.48+1.574ω-0.176ω^2
Peng and Robinson [31]	$\left[1 + f(\omega)\left(1 - \sqrt{T_r}\right)\right]^2$	0.37464+1.54226ω-0.26992ω^2

Table 3: Parameters for Popular Cubic EoS

The general cubic equation of state can be represented as a polynomial, as indicated in Equation 32. In a one-phase region, the fluid is characterized by a single real root, corresponding to the gas, liquid, or supercritical phase. In the two-phase region, a gas-liquid mixture exists, and two roots are identified. The larger root corresponds to the gas phase, while the smaller root pertains to the liquid phase.

$$Z^3-(1+B-uB)Z^2+(A+wB^2-uB-uB^2)Z-AB-wB^2-wB^3 = 0 \tag{32}$$

where $A = \frac{\Phi P}{R^2T^2}$ and $B = \frac{bP}{RT}$.

If the Peng-Robinson equation of state [[31]] is used, the polynomial equation becomes

$$Z^3 - (1 - B)Z^2 + (A - 2B - 3B^2)Z - (AB - B^2 - B^3) = 0 \tag{33}$$

For an ideal gas, the compressibility factor is defined as $Z = 1$, but to describe real-life physical phenomena, the deviation of Z needs to be consider. The value of Z typically increases with pressure and decreases with temperature. At elevated pressures, molecules collide more frequently, allowing repulsive forces between molecules to influence the molar volume of the real gas (v_m) to surpass that of the corresponding ideal gas $\left(\left(v_m\right)_{ideal\ gas} = \frac{RT}{P}\right)$, resulting in Z exceeding one. At lower pressures, molecules move freely, with attractive forces predominating, leading to $Z < 1$.

Numerical methods such as Newton-Raphson can be used to solve the polynomial equation to obtain the compressibility $Z\,(T(t, z), P(t))$ at given temperature and pressure. Alternatively, the closed form solution can by obtained by Cardano formula. Details regarding the Cardano formula can be found in Appendix A.3.

A.1.2. Density of the fluid phase

The density of the fluid can be calculated from the real gas equation $\rho = \frac{P}{RTZ}\frac{1}{m_{CO2}}$. The local temperature can be obtain from the time evolution of governing equations, the pressure is consider to be constant along the system to be a know at any time. The local compressibility factor can be also computed if the local temperature and pressure are know. To obtain the density in terms of mass, molar mass of the solvent is taken into account.

A.1.3. Heat capacity of the fluid phase

The specific heat C_p^{F} can be calculated from the equation of state, under the assumption that the fluid phase consists of pure carbon dioxide and that the specific heat of real fluids can be calculated from an ideal contribution plus a residual term Pratt [32]:

$$C_v = C_v^{id} + C_v^R \tag{34}$$

$$C_p = C_p^{id} + C_p^R \tag{35}$$

The ideal-gas contribution is found using heat-capacity data applicable to gases at very low pressures, which are available in many thermodynamics textbooks in the polynomial form, such as $C_p^{id}(T) = A + BT + CT^2 + DT^3$.

where the coefficients of the expansion are $C_{P0} = 22.26$, $C_{P1} = 5.981 \times 10^{-2}$, $C_{P2} = -3.501 \times 10^{-5}$, and $C_{P3} = 7.469 \times 10^{-9}$, as given by Kyle [33].

The residual component of the specific heat can obtained from general relation between C_v and C_p as given by Poling [34].

$$C_p^R = C_v^R + T\left(\frac{\partial P}{\partial T}\right)_{v_m}\left(\frac{\partial v_m}{\partial T}\right)_P - R \tag{36}$$

The effects of pressure and temperature for liquids are not great, but both C_p and C_v diverge at the critical point of a pure fluid. In the neighborhood of the critical, $\left(\frac{\partial P}{\partial v_m}\right)_T$ approaches zero, so C_p increases much faster than C_v. At both high and low densities, the differences are small, but for T_r near unity, they increase rapidly as the critical density is approached. At fixed density in this region, C_p actually decreases as T increases.

The term $\left(\frac{\partial P}{\partial T}\right)_{v_m}$ can be obtain by direct differentiation of P-R EoS

$$\left(\frac{\partial P}{\partial T}\right)_{v_m} = \frac{R}{v_m - b} - \frac{\frac{d\Phi}{dT}}{\left[v_m(v_m+b)+b(v_m-b)\right]^2} \tag{37}$$

where $\left(\frac{\partial \Phi}{\partial T}\right)_{v_m} = \frac{-f(\omega)a}{\sqrt{TT_c}(1+f(\omega)(1-\sqrt{T/T_c}))}$

The term $\left(\frac{\partial v_m}{\partial T}\right)_P = \frac{R}{P}\left(T\left(\frac{\partial Z}{\partial T}\right)_P + Z\right)$

The term $\left(\frac{\partial Z}{\partial T}\right)_P$ can be defined as below

$$\left(\frac{\partial Z}{\partial T}\right)_P = \frac{\left(\frac{\partial A}{\partial T}\right)_P (B-Z) + \left(\frac{\partial B}{\partial T}\right)_P (6BZ + 2Z - 3B^2 - 2B + A - Z^2)}{3Z^2 + 2(B-1)Z + (A - 2B - 3B^2)} \tag{38}$$

$$\left(\frac{\partial A}{\partial T}\right)_P = (P/(RT)^2)(\frac{d\Phi}{dT} - 2a/T) \tag{39}$$

$$\left(\frac{\partial B}{\partial T}\right)_P = -bP/(RT^2) \tag{40}$$

The first component of Equation 36 from definition of $C_v = \left(\frac{\partial U^R}{\partial T}\right)_{v_m}$, where U^R represents internal energy. In case of Pen-Robinson U^R equals to

$$U^R = \frac{T\frac{d^2\Phi}{dT^2}}{b\sqrt{8}} \ln\left(\frac{Z + B\left(1+\sqrt{2}\right)}{Z + B\left(1-\sqrt{2}\right)}\right) \tag{41}$$

As given by Pratt [32], for Peng-Robinson EoS the term $\frac{d^2\Phi}{dT^2}$ is defined as follow

$$\frac{d^2\Phi}{dT^2} = \frac{af(\omega)\sqrt{\frac{T_c}{T}}\,(1+f(\omega))}{2TT_c} \tag{42}$$

A.1.4. Departure functions for enthalpy calculations

In thermodynamics, a departure function is a concept used to calculate the difference between a real fluid's thermodynamic properties (enthalpy, entropy, or internal energy) and those of an ideal gas, given a specific temperature and pressure. These functions are used to calculate extensive properties, which are properties computed as a difference between two states.

To evaluate the enthalpy change between two points, $h(V_1, T_1)$ and $h(V_2, T_2)$, the enthalpy departure function between the initial volume V_1 and infinite volume at temperature T_1 is calculated. Then it is added to that the ideal gas enthalpy change due to the temperature change from T_1 to T_2, and finally subtract the departure function value between the final volume V_2 and infinite volume.

Departure functions are computed by integrating a function that depends on an equation of state and its derivative. The general form of the enthalpy equation is given by:

$$\frac{h^{id} - h}{RT} = \int_{v_m}^{\infty} \left(T\left(\frac{\partial Z}{\partial T}\right)_{v_m}\right) \frac{dv_m}{v_m} + 1 - Z \tag{43}$$

Here, h^{id} represents the enthalpy of an ideal gas, h is the enthalpy of a real fluid, R is the universal gas constant, T is temperature, v_m is the molar volume, and Z is the compressibility factor.

The integral in the equation is evaluated over the range of molar volumes from v_m to infinity. The integral includes a term that depends on the derivative of the compressibility factor with respect to temperature, evaluated at the molar volume v_m. Finally, the term $1 - Z$ is added to account for the deviation of the fluid's properties from an ideal state.

The Peng–Robinson EoS relates the three interdependent state properties pressure P, temperature T, and molar volume v_m. From the state properties (P, v_m, T), one may compute the departure function for enthalpy per mole (denoted h) as presented by Gmehling et al. [21] or Elliott [7]:

$$h - h^{\mathrm{id}} = RT_c\left[T_r(Z-1) - 2.078(1+\kappa)\sqrt{\alpha}\ln\left(\frac{Z+2.414B}{Z-0.414B}\right)\right] \tag{44}$$

A.2. Governing equations

A.2.1. Mass continuity

Following the work of Anderson [15], the governing equations for compressible fluid with non-uniform cross-section can be obtained. Let's assume that any properties of the flow are uniform across any given cross-section of an extractor. The variation of the cross-section might result from the partial filling of an extractor or its irregular shape. In reality, such a flow is two-dimensional because the area changes as a function of z, and there is a flow-field variation in both directions. The assumption of quasi-one-dimensional flow dictates that the flow properties are a function of z only. The integral form of the continuity equation is:

$$\frac{\partial}{\partial t}\iiint_{\mathcal{V}_f} \rho_f \, d\mathcal{V}_f + \iint_S \rho_f \mathbf{V}\cdot\mathbf{dS} = 0 \tag{45}$$

We apply this equation to the shaded control volume shown in Figure 12.

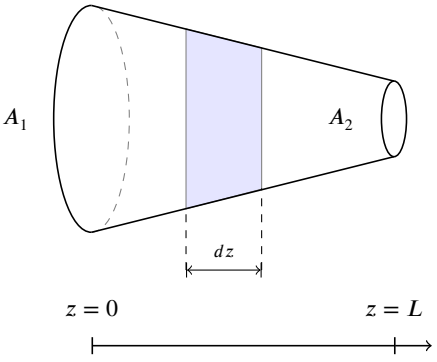

Figure 12: Control volume for deriving the partial differential equation for unsteady, quasi-one-dimensional flow

On the left side of the control volume, consistent with the quasi-one-dimensional assumptions, the density, velocity, pressure, and internal energy denoted by ρ_f, v, P, and e, respectively, are uniform over the area A. Similarly, on the right side of the control volume, the density, velocity,

pressure, and internal energy $\rho_f + d\rho_f$, $v + dv$, $P + dP$, and $e + de$, respectively, are uniform over the area available for fluid phase $A_f + dA_f$. Applied to the control volume in Figure 12, the volume integral in Equation 45 becomes, in the limit as dz becomes very small,

$$\frac{\partial}{\partial t}\iiint_{\mathcal{V}_f} \rho_f d\mathcal{V}_f = \frac{\partial}{\partial t}\left(\rho_f A_f dz\right) \tag{46}$$

where $A\,dz$ is the volume of the control volume in the limit of dz becoming vanishingly small. The surface integral in Equation 45 becomes

$$\iint_S \rho_f \mathbf{V}\cdot\mathbf{dS} = -\rho_f v A_f + (\rho_f + d\rho_f)(v + dv)(A_f + dA_f) \tag{47}$$

The minus sign on the leading term on the right-hand side is due to the vectors $\mathbf{V}$ and $\mathbf{dS}$ pointing in opposite directions over the left of the control volume, and hence the dot product is negative. Expanding the triple product term

$$\begin{aligned}\iint_S \rho_f \mathbf{V}\cdot\mathbf{dS} &= -\rho_f v A_f + \rho_f v A_f + \rho_f v dA_f + \rho_f A_f dv \\ &+ \rho_f dv dA_f + v A_f d\rho_f + v d\rho_f dA + A_f d\rho_f dv + d\rho_f dv dA_f\end{aligned} \tag{48}$$

In the limit as dz becomes very small, the terms involving products of the differential in Equation 48, such as $\rho_f dv dA_f$, $d\rho_f dv dA_f$, go to zero much faster than those terms involving only one differential. Hence, all terms involving products of differentials can be dropped, yielding in the limit as dz becomes very small

$$\iint_S \rho_f \mathbf{V}\cdot\mathbf{dS} = \rho_f v dA_f + \rho_f A_f dv + v A_f d\rho_f \tag{49}$$

Substituting Eqs. 46 and 49 into 45, we have

$$\frac{\partial\left(\rho_f A_f\right)}{\partial t} + \frac{\partial\left(\rho_f A_f v\right)}{\partial z} = 0 \tag{50}$$

The above partial differential equation form of the continuity equation is suitable for unsteady, quasi-one-dimensional flow. The $A_f(z)$ is an arbitrary function that describes a change in the extractor's cross-section and can be defined as $A_f(z) = \mathbf{A}\phi(z)$, where ϕ is the bed porosity and $\mathbf{A}$ is the cross-section of an empty extractor.

$$\frac{\partial\left(\rho_f \mathbf{A}\phi(z)\right)}{\partial t} + \frac{\partial\left(\rho_f \mathbf{A}\phi(z) v\right)}{\partial z} = 0 \tag{51}$$

The equation can be simplified by canceling out a constant $\mathbf{A}$

$$\frac{\partial\left(\rho_f \phi(z)\right)}{\partial t} + \frac{\partial\left(\rho_f \phi(z) v\right)}{\partial z} = 0 \tag{52}$$

If so-called superficial velocity is defined as $u = \phi v$, the mass continuity becomes

$$\frac{\partial\left(\rho_f \phi(z)\right)}{\partial t} + \frac{\partial\left(\rho_f u\right)}{\partial z} = 0 \tag{53}$$

A.2.2. Transport of a species

The transport of a solute, can be described by an analogous equation to the Equation 45 with additional terms on the right-hand side. The first term on the right-hand side describes diffusional movement of species and is based on the Fick's law $\left(J_{diff} = D_e^M \frac{\partial c_f}{\partial z}\right)$. The other term corresponds to the mass transfer between solid and fluid phases, which is treated as a source term.

$$\frac{\partial}{\partial t}\iiint_{\mathcal{V}_f} c_f d\mathcal{V}_f + \iint_S c_f \mathbf{V}\cdot\mathbf{dS} = \iint_S J_{diff}\cdot\mathbf{n}\,\mathbf{dS} + \frac{\partial}{\partial t}\iiint_{\mathcal{V}_s} c_s d\mathcal{V}_s \tag{54}$$

Similarly to the continuity equation, in the limit as dz becomes very small

$$\frac{\partial}{\partial t}\iiint_{\mathcal{V}_f} c_f d\mathcal{V}_f = \frac{\partial}{\partial t}\left(c_f A_f dz\right) \tag{55}$$

$$\frac{\partial}{\partial t}\iiint_{\mathcal{V}_s} c_s d\mathcal{V}_s = \frac{\partial}{\partial t}\left(c_s A_s dz\right) \tag{56}$$

The surface integrals in the limit of dz become

$$\iint_S c_f \mathbf{V}\cdot\mathbf{dS} = c_f v dA_f + c_f A_f dv + v A_f dc_f \tag{57}$$

From the Divergence theorem in multi-variable calculus, we have

$$\iint_S J_{diff}\cdot\mathbf{n}\,\mathbf{dS} = \iiint_{\mathcal{V}_f} \nabla J_{diff} dv_f = \nabla \iiint_{\mathcal{V}_f} J_{diff} dv_f = \nabla\left(J_{diff} A_f dz\right) \tag{58}$$

By substituting the equations derived above into Equation 54 we obtain

$$\frac{\partial\left(c_f A_f\right)}{\partial t} + \frac{\partial\left(c_f A_f v\right)}{\partial z} = \frac{\partial\left(c_s A_s\right)}{\partial t} + \frac{\partial\left(J_{diff} A_f\right)}{\partial z} \tag{59}$$

By defining $A_f = A\cdot\phi$, $A_s = A\cdot(1-\phi)$ and $u = V\cdot\phi$, and assuming that A is constant, the above equation becomes

$$\frac{\partial\left(c_f \phi\right)}{\partial t} + \frac{\partial\left(c_f u\right)}{\partial z} = \frac{\partial\left(c_s(1-\phi)\right)}{\partial t} + \frac{\partial\left(J_{diff}\phi\right)}{\partial z} \tag{60}$$

By assuming that $\frac{\partial\phi}{\partial t} = 0$ and expanding J_{diff}, we get

$$\frac{\partial c_f}{\partial t} + \frac{1}{\phi}\frac{\partial\left(c_f u\right)}{\partial z} = \frac{(1-\phi)}{\phi}\frac{\partial c_s}{\partial t} + \frac{1}{\phi}\frac{\partial}{\partial z}\left(D_e^M \frac{\partial c_f}{\partial z}\right) \tag{61}$$

The equation can be further simplified if $\frac{\partial u}{\partial z} = \frac{\partial\phi}{\partial z} = D_e^M = 0$, which corresponds to the assumptions of constant velocity along the bed(which might be a case of isothermal and low-Mach number flow), constant porosity(which comes from the assumption of constant area for both solid and fluid phase) and no radial diffusion.

$$\frac{\partial c_f}{\partial t} + \frac{u}{\phi}\frac{\partial c_f}{\partial z} = \frac{1-\phi}{\phi}\frac{\partial c_s}{\partial t} \tag{62}$$

The Equation 62 is equivalent to the equation presented by Reverchon [6].

A.2.3. Momentum conservation

Similarly to mass conservation, momentum conservation is derived for inviscid fluid with no body forces

$$\frac{\partial}{\partial t}\iiint_{\mathcal{V}_f} \left(\rho_f v_z\right) d\mathcal{V}_f + \iint_S \left(\rho_f v_z \mathbf{V}\right)\mathbf{dS} = \iint_S (P dS)_z \tag{63}$$

where V_z is the z component of the velocity.

We the momentum conservation to the shaded control volume in Figure 12, the integrals on the left side are evaluated in the same manner as discussed above in the regard to the continuity equation. That is,

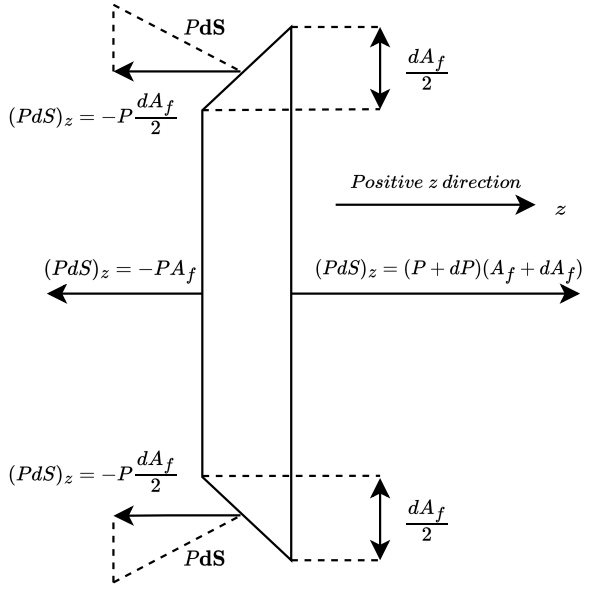

Figure 13: The forces in the z direction acting on the control volume

$$\frac{\partial}{\partial t}\iiint_{\mathcal{V}_f}\left(\rho_f v_z\right)d\mathcal{V}_f = \frac{\partial}{\partial t}\left(\rho_f v A_f dz\right) \tag{64}$$

equation

and

$$\iint_S \left(\rho_f v_z \mathbf{V}\right)dS = -\rho_f v^2 + \left(\rho_f + d\rho_f\right)(v+dv)^2(A+dA) \tag{65}$$

The evaluation of the pressure force term on the right side of Equation 63 can be understood based on the Figure 13. Here, the z components of the vector PdS are shown on all four sides of the control volume. Remember that **dS** is assumed to point away from the control volume; hence any z component $(PdS)_z$ that acts toward the left (in the negative z direction) is a negative quantity. Any z component that acts toward the right (in the positive z direction) is a positive quantity. Also note that the z component of **PdS** acting on the top and the bottom inclined faces of the control volume in Figure 13 can be expressed as the pressure P acting on the component of the inclined is projected perpendicular to the z direction, $dA_f/2$; hence, the contribution of each inclined face (top or bottom) to the pressure integral in Equation 63 is $-P(dA_f/2)$. All together, the right-hand side of Equation 63 is expressed as follows:

$$\iint (PdS)_z = -PA_f + (P+dP)(A+dA_f) - 2P\frac{dA_f}{2} \tag{66}$$

Substituting Eqs. 64 to 66 into Equation 63, we have

$$\begin{aligned}&\frac{\partial}{\partial t}\left(\rho_f v A_f dz\right) - \rho_f v^2 A_f + (\rho_f + d\rho_f)(v+dv)^2(A_f+dA_f)\\ &= PA_f - (P+dP)(A+dA_f) + PdA_f\end{aligned} \tag{67}$$

Canceling like terms and ignoring products of differentials, the equation above becomes in the limit dz becoming very small

$$\frac{\partial}{\partial t}\left(\rho_f v A_f dz\right) + d\left(\rho_f v^2 A_f\right) = -AdP \tag{68}$$

Dividing the above equation by dz and taking the limit as dz goes to zero, we obtain

$$\frac{\partial\left(\rho_f v A_f\right)}{\partial t} + \frac{\partial\left(\rho_f v^2 A_f\right)}{\partial z} = -A_f\frac{\partial P}{\partial z} \tag{69}$$

The Equation 69 can be expanded further by assuming that $A_f = \mathbf{A}\phi$

$$\frac{\partial\left(\rho_f v \mathbf{A}\phi\right)}{\partial t} + \frac{\partial\left(\rho_f v^2 \mathbf{A}\phi\right)}{\partial z} = -\mathbf{A}\phi\frac{\partial P}{\partial t} \tag{70}$$

The equation can be further simplified by assuming that the cross-section of an extractor $\mathbf{A}$ is constant and cancel out

$$\frac{\partial\left(\rho_f v\phi\right)}{\partial t} + \frac{\partial\left(\rho_f v^2\phi\right)}{\partial z} = -\phi\frac{\partial P}{\partial t} \tag{71}$$

If the superficial velocity $u = \phi V$ is introduced, then the momentum conservation becomes

$$\frac{\partial\left(\rho_f u\right)}{\partial z} + \frac{\partial\left(\rho_f u^2/\phi\right)}{\partial z} = -\phi\frac{\partial P}{\partial z} \tag{72}$$

Equation 69 represents the conservative form of the momentum equation for the quasi-one-dimensional flow. The equivalent non-conservative form can be obtained by multiplying the continuity equation by v and subtracting it from Equation 69

$$\frac{\partial\left(\rho_f v A_f\right)}{\partial t} - V\frac{\partial\left(\rho_f A_f\right)}{\partial t} + \frac{\left(\rho_f v^2 A_f\right)}{\partial z} - V\frac{\left(\rho_f v A_f\right)}{\partial z} = -A_f\frac{\partial P}{\partial z} \tag{73}$$

Expanding the derivatives on the left-hand side of the above equation and canceling like terms, gives

$$\rho_f A_f\frac{\partial v}{\partial t} + \rho_f A_f v\frac{\partial v}{\partial z} = -A_f\frac{\partial P}{\partial z} \tag{74}$$

Dividing the above equation by A_f the non-conservative form of the momentum can be obtained

$$\rho_f\frac{\partial v}{\partial t} + \rho_f v\frac{\partial v}{\partial z} = -\frac{\partial P}{\partial z} \tag{75}$$

The Equation 75 is stylistically the same as the general momentum conservation for one-dimensional flow with no-body forces. The momentum equation can be expressed in terms of superficial velocity $u = v\phi$.

$$\rho_f\frac{\partial\left(u/\phi\right)}{\partial t} + \rho_f\frac{u}{\phi}\frac{\partial\left(u/\phi\right)}{\partial z} = -\frac{\partial P}{\partial z} \tag{76}$$

By expanding all the terms of the equation above, we get

$$\frac{\rho_f}{\phi}\frac{\partial u}{\partial t} + \rho_f u\frac{\partial\phi^{-1}}{\partial t} + \rho_f\frac{u}{\phi}\frac{1}{\phi}\frac{\partial u}{\partial z} + \rho_f\frac{u}{\phi}u\frac{\partial\phi^{-1}}{\partial z} = -\frac{\partial P}{\partial z} \tag{77}$$

If the bed is not compressible and doesn't change its properties during the batch, then $\dfrac{\partial\phi}{\partial t} = 0$

$$\frac{\rho_f}{\phi}\left(\frac{\partial u}{\partial t} + \frac{u}{\phi}\frac{\partial u}{\partial z} + u^2\frac{\partial\phi^{-1}}{\partial z}\right) = -\frac{\partial P}{\partial z} \tag{78}$$

If the porosity is constant along an extractor, then the momentum conservation equation becomes

$$\frac{\rho_f}{\phi}\left(\frac{\partial u}{\partial t} + \frac{u}{\phi}\frac{\partial u}{\partial z}\right) = -\frac{\partial P}{\partial z} \tag{79}$$

The Equation 79 represents the non-conservative form of the momentum equation for quasi-one-dimensional flow with no body forces and constant porosity.

A.2.4. Energy conservation

Let's consider the integral form of the energy equation for adiabatic flow with no body forces and no viscous effects

$$\frac{\partial}{\partial}\iiint_{\mathcal{V}_f}\rho_f\left(e_f+\frac{v^2}{2}\right)d\mathcal{V}_f+\iint_S\rho_f\left(e_f+\frac{v^2}{2}\right)\mathbf{V}\cdot\mathbf{dS}=-\iint_S(P\mathbf{V})\cdot\mathbf{dS} \tag{80}$$

Applied to the shaded control volume in Figure 12, and keeping in mind the pressure forces shown in Figure 13, Equation 80 becomes

$$\begin{aligned}&\frac{\partial}{\partial t}\left[\rho_f\left(e_f+\frac{v^2}{2}\right)A_f dz\right]-\rho_f\left(e_f+\frac{v^2}{2}\right)vA_f\\&+\left(\rho_f+d\rho_f\right)\left[e_f+de_f+\frac{(v+dv)^2}{2}\right](V+dV)\left(A_f+dA_f\right)\\&=-\left[-PvA_f+(P+dP)(v+dv)\left(A_f+dA_f\right)-2\left(Pv\frac{dA_f}{2}\right)\right]\end{aligned} \tag{81}$$

Neglecting products of differential and canceling like terms, the above equation becomes

$$\frac{\partial}{\partial t}\left[\rho_f\left(e_f+\frac{v^2}{2}\right)A_f dz\right]+d\left(\rho_f r_f A_f\right)+\frac{\left(\rho_f v^3 A_f\right)}{2}=-d\left(PA_f v\right) \tag{82}$$

or

$$\frac{\partial}{\partial t}\left[\rho_f\left(e_f+\frac{v^2}{2}\right)A_f dz\right]+d\left[\rho_f\left(e_f\frac{v^2}{2}\right)vA_f\right]=-d\left(PA_f v\right) \tag{83}$$

Taking the limit as dz approaches zero, the equation above becomes the following partial differential equation

$$\frac{\partial\left[\rho_f\left(e_f+v^2/2\right)A\right]}{\partial t}+\frac{\partial\rho_f\left(e_f+v^2/2\right)vA_f}{\partial z}=-\frac{\partial\left(PA_f v\right)}{\partial z} \tag{84}$$

Equation 84 is the conservation form of the energy expressed in terms of the total energy $e+v^2/2$, appropriate for unsteady, quasi-one-dimensional flow. The energy equation can be expressed in terms of internal energy if Equation 69 is multiplicated by v and then subtracted from Equation 84

$$\frac{\partial\left(\rho_f e_f A_f\right)}{\partial t}+\frac{\partial\left(\rho_f e_f vA_f\right)}{\partial z}=-P\frac{\partial A_f v}{\partial z} \tag{85}$$

The equation above is the conservation form of the energy equation expressed in terms of internal energy e_f suitable for quasi-one-dimensional flow. The non-conservative for is then obtained by multiplying the continuity equation 50, by e_f and substructing it from 85, yielding

$$\rho_f A_f\frac{\partial e_f}{\partial t}+\rho_f A_f v\frac{\partial e_f}{\partial z}=-P\frac{\partial(A_f v)}{\partial z} \tag{86}$$

Expanding the right-hand side and dividing by A_f, the above equation becomes

$$\rho_f\frac{\partial e_f}{\partial t}+\rho_f v\frac{\partial e_f}{\partial z}=-P\frac{v}{A_f}\frac{\partial A_f}{\partial z} \tag{87}$$

or

$$\rho_f\frac{\partial e_f}{\partial t}+\rho_f v\frac{\partial e_f}{\partial z}=-P\frac{\partial v}{\partial z}-PV\frac{\partial(ln\ A_f)}{\partial z} \tag{88}$$

Equation 88 is the non-conservative form of the energy equation expressed in terms of internal energy, appropriate to unsteady quasi-one-dimensional flow. The reason for obtaining the energy equation in the form of Equation 88 is that, for a calorically perfect gas, it leads directly to a form of the energy equation in terms of temperature T.

A.3. Cardano's Formula

Following the work of Gmehling et al. [21], a cubic equation of state can be written a following form

$$Z^3+UZ^2+SZ+T=0 \tag{89}$$

with Z as the compressibility factor. Using Cardano's formula, this type of equation can be solved analytically. With the abbreviations

$$P=\frac{3S-U^2}{3}\qquad Q=\frac{2U^3}{27}-\frac{US}{3}+T$$

the discriminant can be determined to be

$$D=\left(\frac{P}{3}\right)^3+\left(\frac{Q}{2}\right)^2 \tag{90}$$

For $D>0$, the equation of state has one real solution:

$$Z=\left[\sqrt{D}-\frac{Q}{2}\right]^{1/3}-\frac{P}{3\left[\sqrt{D}-\frac{Q}{2}\right]^{1/3}}-\frac{U}{3} \tag{91}$$

For $D<0$, there are three real solutions. With the abbreviations

$$\Theta=\sqrt{-\frac{P^3}{27}}\qquad\Phi=\arccos\left(\frac{-Q}{2\Theta}\right)$$

they can be written as

$$Z_1=2\Theta^(1/3)\cos\left(\frac{\Phi}{3}\right)-\frac{U}{3} \tag{92}$$

$$Z_2=2\Theta^(1/3)\cos\left(\frac{\Phi}{3}+\frac{2\pi}{3}\right)-\frac{U}{3} \tag{93}$$

$$Z_3=2\Theta^(1/3)\cos\left(\frac{\Phi}{3}+\frac{4\pi}{3}\right)-\frac{U}{3} \tag{94}$$

The largest and the smallest of the three values correspond to the vapor and to the liquid solutions, respectively. The middle one has no physical meaning.

A.4. Maximum likelihood

Maximum likelihood estimation (MLE) is a statistical method used to estimate the parameters of a probability distribution based on observed data. The MLE works by finding the values of the parameters that maximize the likelihood function, which is the probability of observing the given data for a given set of parameter values. The MLE has desirable properties such as asymptotic efficiency and normality. Although the MLE has often been associated with the normal distribution for mathematical convenience, it can be applied to a wide range of probability distributions.

To find the maximum likelihood estimates, we maximize the joint probability density function, or likelihood function, denoted as $p(\theta|y(t_1),y(t_2),...,y(t_n))$, where θ represents the parameters and $y(t_1),y(t_2),...,y(t_n)$ represent the observed data. The conditions at the maximum can be refined by incorporating prior information. The posterior probability density function $p(\theta|y)$ can be expressed as the ratio of two probability densities using the continuous variable analogue of Bayes' theorem . In such a case the posteriori distribution is given by Equation 95.

$$p\left(\theta|y(t_n),...,y(t_1)\right)=\frac{p\left(\theta,y(t_n),...,y(t_1)\right)}{p\left(y(t_n),...,y(t_1)\right)} \tag{95}$$

The numerator of the right-hand side od Equation 95 becomes

$$\begin{aligned}p\left(\theta,y(t_n),...,y(t_1)\right)&=p\left(y(t_n)|\theta,y(t_{n-1}),...,y(t_1)\right)\\&\cdot p\left(\theta,y(t_{n-1}),...,y(t_1)\right)\end{aligned} \tag{96}$$

These operations can be continued repetitively until we get

$$p\left(\theta,y(t_n),...,y(t_1)\right)=p\left(\theta\right)\prod_{i=1}^{n}p\left(y(t_i)|\theta,y(t_{i-1}),...,y(t_1)\right) \tag{97}$$

Examination of Equation 28 shows that $dY(t_i)/dt$ depends only on t_i, θ and $\epsilon(t_i)$ and is not conditioned by any previous measurement. Consequently, we can write

$$p\left(y(t_i)|\theta,y(t_{i-1}),...,y(t_1)\right)=p\left(y(t_i)|\theta\right) \tag{98}$$

provided Equation 28 is observed as a constraint. The desired joint conditional probability function is thus

$$p\left(\theta|y(t_n),...,y(t_1)\right)=\frac{p\left(\theta\right)\prod_{i=1}^{n}p\left(y(t_i)|\theta\right)}{p\left(y(t_n),...,y(t_1)\right)} \tag{99}$$

We can get rid of the evidence term $p\left(y(t_n),...,y(t_1)\right)$ because it's constant with respect to the maximization. Moreover, if we are lacking a prior distribution over the quantity we want to estimate, then $p(\theta)$ can be omitted. In such a case:

$$p\left(\theta|y(t_n),...,y(t_1)\right)=\prod_{i=1}^{n}p\left(y(t_i)|\theta\right)=\prod_{i=1}^{n}L\left(\theta|y(t_i)\right) \tag{100}$$

The likelihood function $L\left(\theta|y\right)$ for the parameters based on several observations is the product of the individual functions if the observations are independent.

$$\begin{aligned}L\left(\theta|y(t_n),...,y(t_1)\right)&=\prod_{i=1}^{n}L\left(\theta|y(t_i)\right)\\&=p\left(y(t_1)|\theta\right)p\left(y(t_2)|\theta\right)...p\left(y(t_n)|\theta\right)\end{aligned} \tag{101}$$

In choosing as estimates of θ the values that maximize L for the given values $\left(y(t_i)\right)$, it turns out that it is more convenient to work with the $\ln L$ than with L itself:

$$\ln L=\ln p\left(y(t_1)|\theta\right)+\ln p\left(y(t_2)|\theta\right)+...+\ln p\left(y(t_n)|\theta\right)=\sum_{i=1}^{n}\ln p\left(y(t_i);\theta\right) \tag{102}$$

By assuming that the conditional distribution of $\bar{Y}_i$, given y_i, is normal, then we form the likelihood function based on the probability density:

$$\begin{aligned}p\left(\theta,\sigma|y(t_n),...,y(t_1)\right)&=\prod_{i=1}^{n}\frac{1}{\sqrt{2\pi}\sigma}\exp\left[\frac{1}{2\sigma}\left(Y(t_i)-y(\theta,t_i)\right)^2\right]\\L\left(\theta,\sigma|y(t_n),...,y(t_1)\right)&=\prod_{i=1}^{n}\frac{1}{\sqrt{2\pi}\sigma}\exp\left[\frac{1}{2\sigma}\left(Y(t_i)-y(\theta,t_i)\right)^2\right]\end{aligned} \tag{103}$$

where σ is the variance

By taking the natural logarithm of the Equation 103, the final form of the objective function can be obtained:

$$\ln L=-\frac{n}{2}\left(\ln\left(2\pi\right)+\ln\sigma^2\right)-\frac{\sum_{i=1}^{n}\left[Y(t_i)-y(\theta,t_i)\right]^2}{2\sigma^2} \tag{104}$$